Reviewed Preprint
v1 • April 15, 2026
Not revised

Reviewed Preprint
v2 • June 17, 2026
Revised by authors

For correspondence:
ymchai@ustc.edu.cn
qwen@ustc.edu.cn

* Equal contribution

Competing interests: No competing interests declared

Funding: See page 27

Reviewing editor: Mariano Soiza-Reilly, Universidad de Buenos Aires - CONICET, Argentina

Serotonergic modulation of motor subspace dynamics drives a sleep-independent quiescent state

Kexin Qi[1,2,*], Yuming Chai[1,2,*] ✉, Guodong Tan[1,2], Daguang Li[1,2], Quan Wen[1,2,3] ✉

[1]Division of Life Sciences and Medicine, University of Science and Technology of China, Hefei, China • [2]Hefei National Laboratory for Physical Sciences at the Microscale, Center for Integrative Imaging, University of Science and Technology of China, Hefei, China • [3]School of Data Science, University of Science and Technology of China, Hefei, China

eLife Assessment

In light of the diverse functions associated with the Dorsal Raphe Nucleus across vertebrate species, this **important** study presents findings on the role of serotonin in promoting behavioral quiescence through the regulation of neuromotor populations. Combining optogenetics with brain-wide activity analyses, the study provides **convincing** evidence of interest to researchers in neuromodulation and translational medicine fields.

https://doi.org/10.7554/eLife.110370.2.sa3

Abstract

The dorsal raphe nucleus (DRN) serotonergic (5-HT) system has been implicated in regulating sleep and motor control; however, its specific role remains controversial. In this study, we found that optogenetic activation of DRN 5-HT neurons in larval zebrafish induced a quiescent state and a reduced response to acoustic stimuli. Unlike sleep, the induced quiescent state was not accompanied by a loss of postural control, and nighttime activation of DRN 5-HT neurons led to a subsequent sleep rebound. Whole brain light field imaging combined with demixed principal component analysis (dPCA) revealed distinct neural subspaces related to DRN activation, sound responses, and motor activity. DRN 5-HT activation selectively modulated the motor-related subspace while leaving the sound-evoked subspace unaffected. Unlike DRN activation, sleep induced by mepyramine significantly altered sound-evoked neuronal activity patterns. Further analysis demonstrated that serotonin had a graded effect on the motor subspace, wherein downstream neurons responsible for particular bout types were more significantly influenced. Embedding motor population activity in a curved geometric space revealed that the degree of curvature scales with behavioral suppression across animals, providing a quantitative signature of the quiescent state. Together, these results elucidate that serotonergic modulation promotes behavioral quiescence through selective regulation of motor populations.

Introduction

Serotonin (5-hydroxytryptamine, 5-HT), known as the “feel-good” molecule, is a key monoaminergic neurotransmitter that exerts an expansive influence across the central nervous system (1–6), regulating essential physiological and behavioral processes such as locomotion (7–15), sleep (16–20), emotion (21–23), and learning (24–28). Within the vertebrate brain, the dorsal raphe nucleus (DRN) serves as the primary hub for serotonergic synthesis, providing the dominant source of ascending serotonin to widespread brain regions (2, 29). The DRN 5-HT system has long been implicated in the regulation of sleep and arousal; yet, its precise contribution to the sleep–wake cycle remains one of the most enduring enigmas in neurobiology (19, 30, 31). For more than half a century, a central controversy has persisted: whether serotonergic signaling functions as a primary driver of sleep induction or as a promoter of cortical arousal (16, 17, 19, 30–34).

The larval zebrafish (*Danio rerio*) provide an excellent model for reconciling these conflicting perspectives. They exhibit well-defined sleep behavior, characterized by reduced locomotor activity, sustained immobility, elevated arousal thresholds, and homeostatic sleep rebound following sleep deprivation (35–41). The zebrafish serotonergic system is highly conserved with mammals in anatomy and function (18, 42–44). The small size and optical transparency of the larval zebrafish brain enable whole-brain, cellular-resolution imaging, offering a unique opportunity to dissect serotonergic modulation across the entire neural population.

In zebrafish, increased DRN 5-HT neuron activity is often associated with locomotor suppression, suggesting that serotonergic signaling promotes sleep. Optogenetic activation of these neurons induces sleep-like behavior, while their ablation disrupts sleep-promoting pathways(18, 20), supporting a sleep-promoting role. Yet several lines of evidence suggest the opposite. Electrophysiological recordings show that DRN 5-HT neurons fire at higher rates during the day than at night (18), which is the opposite of the sleep rhythm, indicating a wake-related component of serotonergic activity. Transient water-flow stimulation and exposure to conspecific alarm substances both enhance DRN 5-HT neuron activity and sensory responsiveness, even when locomotion is suppressed (44, 45).

Beyond arousal and sleep, DRN 5-HT neurons are consistently more active in behavioral states with reduced locomotion. During exploitation in naturalistic foraging, zebrafish exhibit decreased movement, increased predation, and elevated DRN activity (46). DRN 5-HT neurons are essential for motor adaptation under visuomotor mismatch, where higher 5-HT levels correlate with reduced tail movements and reticulospinal excitability (47–50). These findings indicate that serotonergic activity is tightly linked to locomotor suppression across diverse behavioral contexts.

These seemingly contradictory studies pose a central question: How do changes in serotonin levels modulate an animal's internal state and behavior, such that they either produce enhanced sensitivity to external stimuli, as in vigilance, or reduced sensitivity, as in sleep? We address this using a custom all-optical system for simultaneous optogenetic manipulation of DRN 5-HT neurons and whole-brain calcium imaging in behaving larval zebrafish. Zebrafish spontaneously alternate between locomotor and quiescent states, with DRN activity markedly elevated during quiescence. Optogenetic activation of DRN 5-HT neurons induced behavioral quiescence and reduced responsiveness to acoustic stimuli, in a state distinct from natural sleep. Whole-brain light-field imaging with demixed principal component analysis (dPCA) revealed separate neural subspaces associated with DRN activation, auditory processing, and motor activity. Our findings reveal that serotonergic modulation promotes behavioral quiescence through hierarchical control of motor circuits without altering auditory stimulus encoding, elucidating how the 5-HT system shapes brain states and behavioral flexibility.

Results

DRN 5-HT activation creates a quiescent, non-sleep state

We developed a custom optical system (51) for stable, long-term whole-brain imaging, tracking, and targeted optogenetic stimulation in freely swimming larval zebrafish (Fig. 1A). We recorded 60-minute spontaneous behavior and brain-wide neural activity in *elavl3:H2B-jGCaMP8s* transgenic larvae. The fish alternated naturally between locomotor and quiescent states (Fig. 1B). Consistent with previous work (46), whole-brain imaging revealed sustained and elevated DRN neuronal activity during the quiescent state (Fig. 1C, Fig. 1D). We then optogenetically activated DRN serotonergic neurons in the *Tg(tph2:ChrimsonR-mKate2)* transgenic fish (Fig. 2A). Although the *tph2* promoter primarily drives expression in DRN 5-HT neurons, minor expression in the pineal gland of the forebrain was minimized by spatially restricting 588 nm laser stimulation to the DRN (30 μW, 50 Hz galvo scanning, Fig. 1A). Each 5-min stimulation was repeated 2–4 times per fish. DRN activation markedly suppressed locomotor activity, inducing a near-quiescent state, whereas control fish lacking ChrimsonR showed no effect (Fig. 2B). Low-frequency optogenetic stimulation also produced a similar reduction in locomotor activity (Fig. S1A-B).

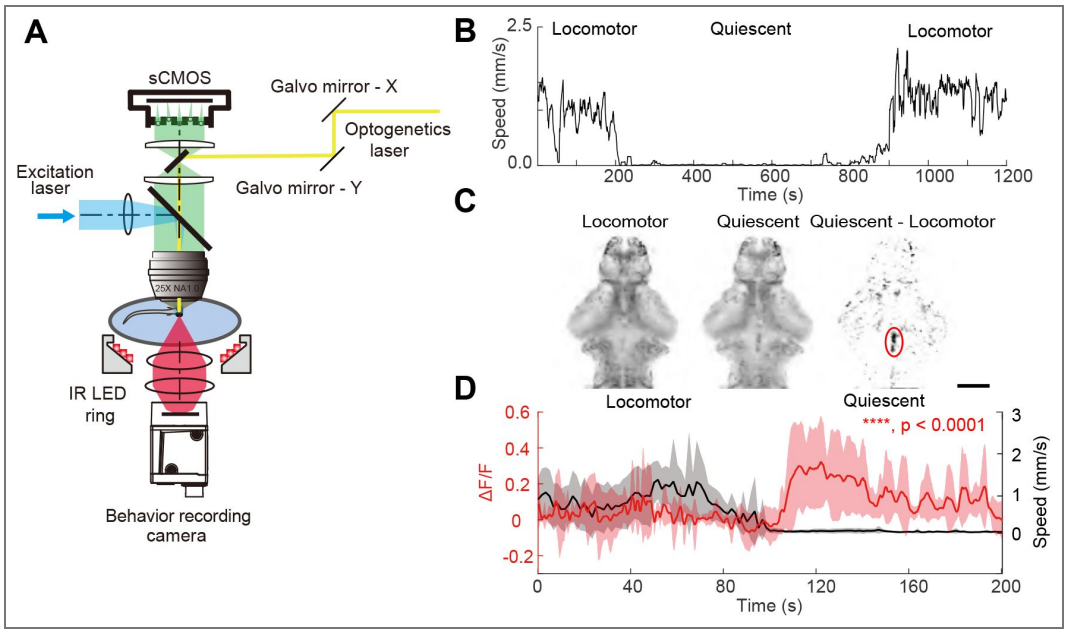

Figure 1. DRN neuronal activity increased during quiescence.

A. A schematic of our all-optical system that integrates tracking, dual-color volumetric fluorescence imaging, and optogenetic manipulation. **B**. Example zebrafish exhibited alternating locomotor and quiescent states during spontaneous behavior. **C**. Maximum intensity projection (MIP) of whole-brain imaging in a zebrafish, showing 30 s averaged neural activity during locomotor (left) and quiescent (middle) states; their difference is shown on the right. The red circle marks the dorsal raphe nucleus (DRN). Scale bar, 100 μm. **D**. Relationship between locomotor speed and DRN neural activity. Data are mean ± SD, n = 5 fish, $p < 0.0001$ (Mann–Whitney U test).

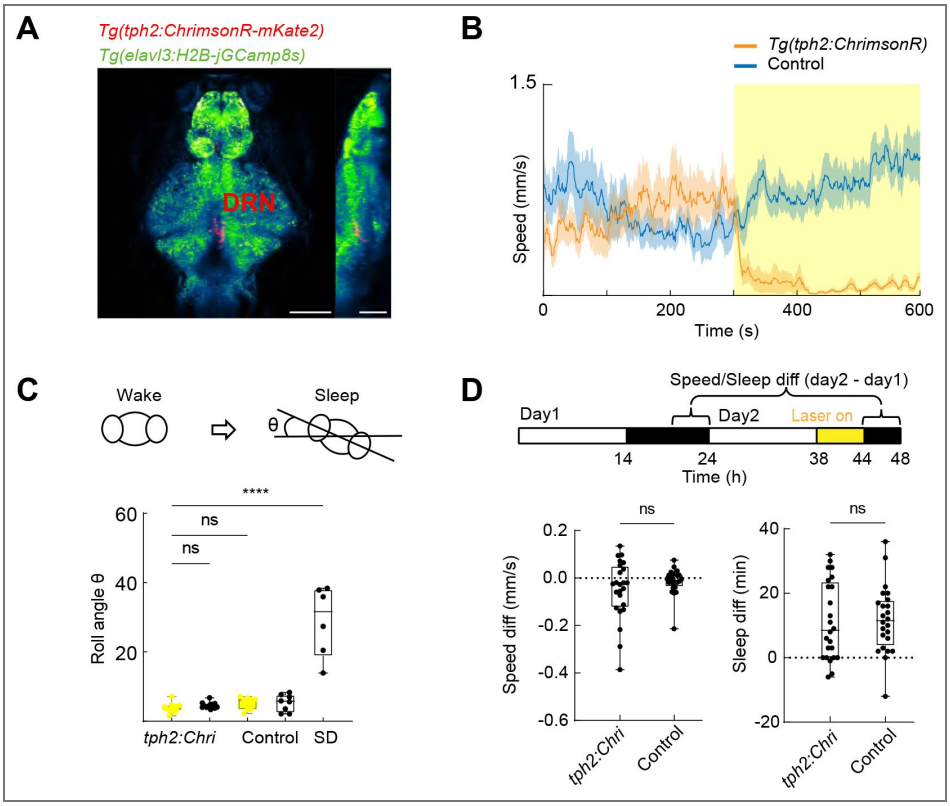

Figure 2. DRN 5-HT activation induces a quiescent but non-sleep-like state.

A. MIP of whole-brain data from a 7 dpf *Tg(tph2:ChrimsonR-mKate2* × *elavl3:h2b-jGCaMP8s)* zebrafish acquired by two-photon microscopy. Scale bar, 100 *μ*m. **B**. Locomotor velocity changes in *Tg(tph2:ChrimsonR)* and control zebrafish during DRN 5-HT neuron activation (n = 6). Yellow shading marks optogenetic stimulation. **C**. Top: Body roll angle (rotation in the Y–Z plane) increases during natural sleep, indicating loss of postural stability. Body roll angle in control (n = 8), sleep-deprived (SD, n = 6), and *Tg(tph2:ChrimsonR)* zebrafish (n = 12). Yellow indicates optogenetic stimulation. In *Tg(tph2:ChrimsonR)* fish, light versus no-light conditions were compared with the Wilcoxon matched-pairs signed rank test. *Tg(tph2:ChrimsonR)* versus control and sleep-deprived versus *Tg(tph2:ChrimsonR)* were compared with the Mann–Whitney U test. ****p < 0.0001. **D**. Top: Experimental timeline over two light–dark cycles (14 h light/10 h dark). The first cycle was normal; in the second, optogenetic stimulation was applied during the first 6 h of the dark period. Average locomotor speed and sleep duration in the 4 h after stimulation were compared with the corresponding 4 h of the first dark period. Bottom: Differences in average locomotor speed and sleep duration between *Tg(tph2:ChrimsonR)* (n = 24) and control zebrafish (n = 24), analyzed with the Mann–Whitney U test.

Optogenetic activation of DRN 5-HT neurons suppressed locomotion in freely swimming zebrafish. This effect has been interpreted as either promoting sleep (18) or vigilance-related immobility (44). To test whether this quiescence resembles sleep, we examined postural control. Unlike natural sleep, which causes postural instability and increased roll angles(52), DRN 5-HT activation did not significantly alter roll angles, whereas sleep-deprived (SD) zebrafish showed clear instability during quiescence (Fig. 2C, Fig. S1C-D). We next tested whether DRN activation during the dark (sleep) phase would block sleep rebound: if this quiescent state were sleep, no rebound would be expected. Instead, stimulation led to a rebound comparable to controls (Fig. 2D, Fig. S1E-F). Together, these results suggest that DRN activation induces a quiescent but non-sleep state in larval zebrafish.

DRN 5-HT activation modulates brain state

To assess how optogenetic activation of DRN 5-HT neurons alters global neural dynamics, we applied demixed principal component analysis (dPCA) to whole-brain activity data (53). dPCA decomposes population activity into components associated with specific experimental variables, enabling the isolation of DRN-dependent effects. To minimize direct optogenetic effects on the identified subspace, DRN-localized regions were excluded from the analysis (Methods).

Within this analysis framework, each dPCA component can be interpreted as a direction in population activity space along which neural activity varies with a given variable (e.g., optogenetic activation). Projecting population activity onto this axis yields a low-dimensional trajectory that captures how this variable modulates neural dynamics over time (Fig. S2). The strength of modulation can be quantified as the fraction of variance associated with the variable that is explained by the components, and neurons with larger weights contribute more strongly to this variable-related activity.

Components associated with DRN activation explained significantly more variance in *Tg(tph2:ChrimsonR)* zebrafish than in controls (Fig. 3A), indicating a strong serotonergic impact on brain-wide neural activity. The small stimulation-related variance in controls likely reflected visual responses to the laser. Projection of whole-brain activity onto the first demixed principal component (dPC1 score), which accounted for over half of the data variance (Fig. 3A), revealed a pronounced and reversible state transition during DRN activation (Fig. 3B). Brain regions with high dPC1 weights (Fig. 3C) showed activity more strongly correlated with locomotor behavior than randomly selected regions (Fig. 3D and Method). Thus, DRN 5-HT activation rapidly reorganizes global neural states and selectively engages motor-related circuits.

DRN 5-HT activation modulates motor circuits to suppress sound-evoked responses

Across species, sleep features an increased arousal threshold and reduced responsiveness to external stimuli (54). In contrast, a recent study shows that DRN 5-HT neuron activation enhances zebrafish vigilance to aversive cues (44), lowering the auditory response threshold – an effect opposite to the sleep-promoting effect of DRN activation (18). To test how DRN 5-HT neurons regulate behavioral states, we present auditory stimuli during DRN activation. Based on larval auditory sensitivity (55), a 350 Hz pure tone (500 ms, 100 dB) was delivered every 60 s (Fig. 4A). *Tg(tph2:ChrimsonR)* larvae exhibited strong locomotor suppression and near-complete loss of sound-evoked escape responses during stimulation (Wilcoxon matched-pairs signed rank test, **p = 0.0039), both of which recovered afterwards (Fig. 4B). Control fish showed no significant changes in swimming speed or escape probability but displayed weak habituation across trials (Fig. 4B, (56)).

To examine how DRN 5-HT neuron activation affects sensorimotor processing (Fig. 4C), we next recorded whole-brain neural activity in head-fixed, tail-free larvae embedded in agarose to capture transient calcium signals with minimal motion artifacts. dPCA revealed neural subspaces associated with auditory processing, motor activity, and DRN 5-HT activation (Fig. 4D, Fig.

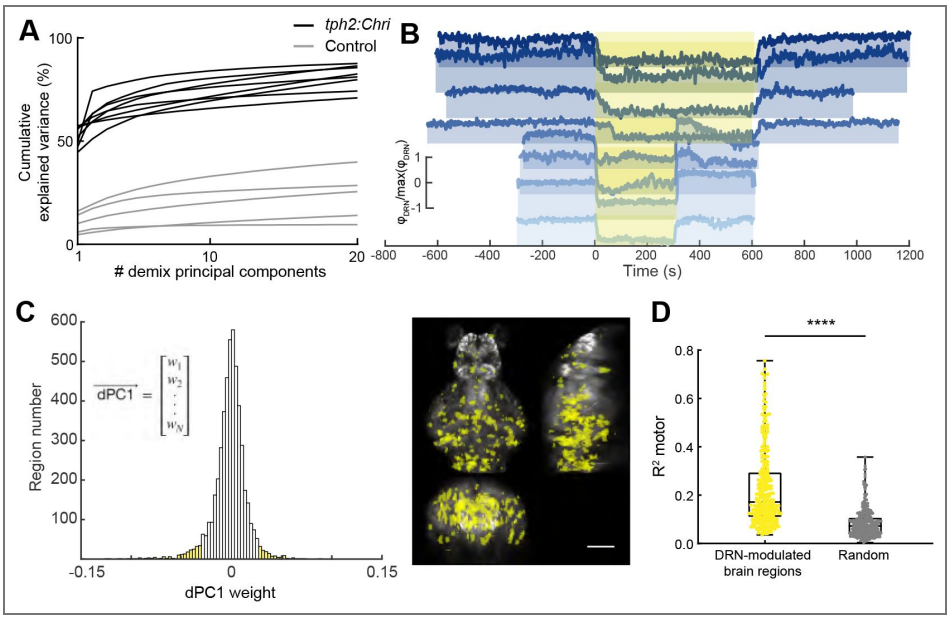

Figure 3. DRN 5-HT activation modulates brain state.

A. Cumulative variance explained by demixed principal components (dPCs) related to optogenetic stimulation in *Tg(tph2:ChrimsonR)* zebrafish (n = 8) and controls (n = 5). **B**. Time course of whole-brain activity projected onto dPC1 in *Tg(tph2:ChrimsonR)* zebrafish (n = 8). Yellow shading marks optogenetic stimulation. *ΦDRN* represents dPC1 score. **C**. Left: Histogram of brain-region weight distribution in dPC1. Yellow shading highlights high-weight regions (|weight| > 0.03, 272 regions). Right: Spatial distribution of these regions in the zebrafish brain. Scale bar, 100 μm. **D**. R^2 between neural activity in dPC1 high-weight regions and locomotor behavior, compared with randomly selected regions (n = 272; Mann–Whitney U test, ****p<0.0001).

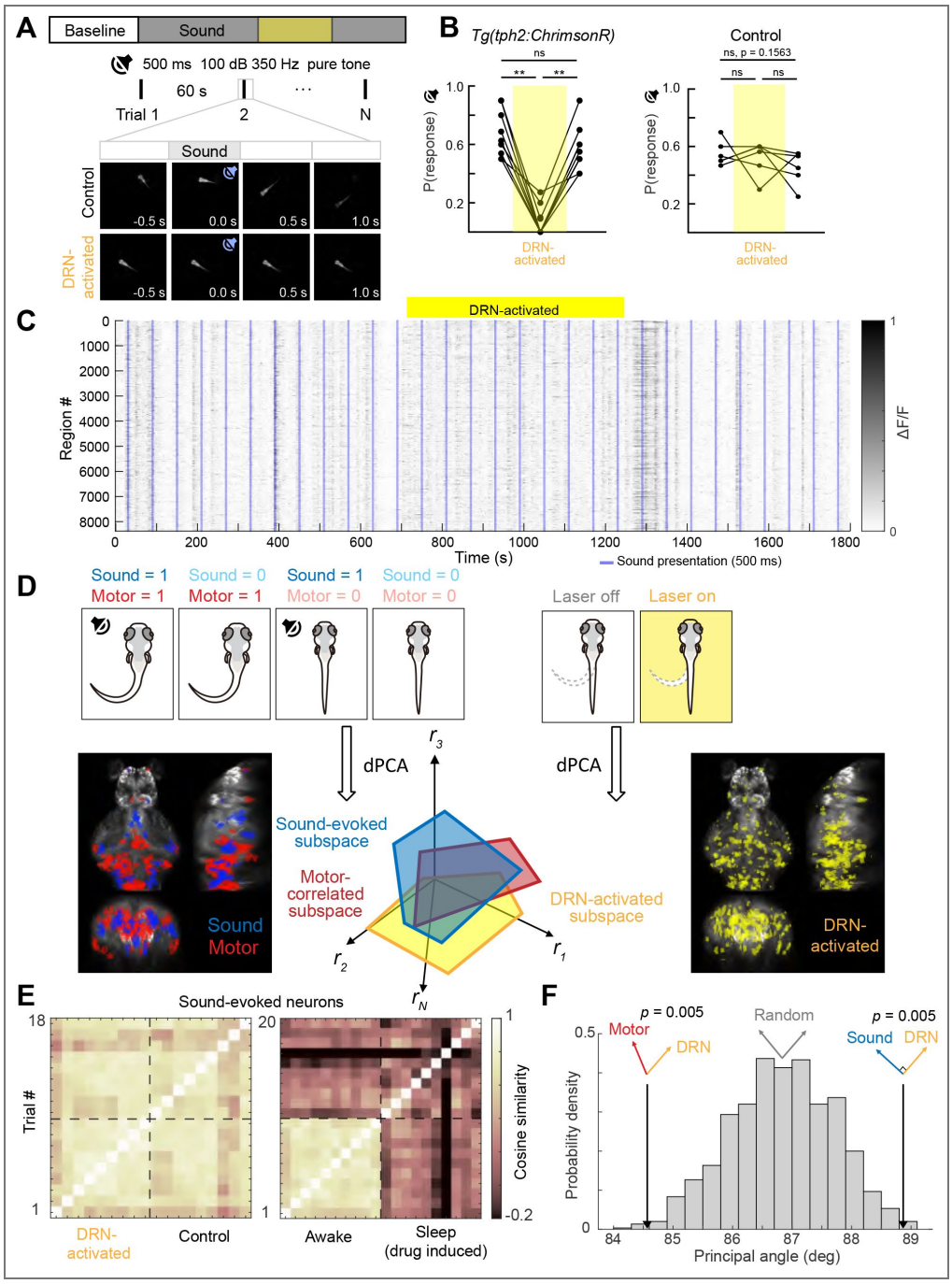

Figure 4. DRN 5-HT activation modulates motor circuits to reduce sound-evoked responses.

A. Experimental protocol for sound stimulus experiments. **B**. Probability of sound-evoked escape in *Tg(tph2:ChrimsonR)* and control zebrafish before, during, and after optogenetic stimulation. Yellow shading marks optogenetic activation. Wilcoxon matched-pairs signed rank test, **p = 0.0039. **C**. Population raster plot of simultaneously recorded neurons during DRN 5-HT activation and control. Blue lines mark sound onset. **D**. Schematic of sound, motor, and DRN activation subspaces identified by dPCA. Left and right MIPs show brain regions with high weights in each subspace in an example zebrafish (bottom right panel is the same as the panel shown in Figure 3C). **E**. Left: Similarity matrix of sound-evoked population responses during DRN activation vs. control. Right: Same analysis comparing awake and drug-induced sleep. **F**. Principal angle analysis shows the motor subspace is significantly aligned with the DRN activation subspace, while the sound subspace is nearly orthogonal (p-values from a nonparametric permutation test, 1000 iterations). Arrows show the mean angle, across all fish, between the DRN 5-HT activation subspace and the motor-related subspace (left) or the sound-related subspace (right). "Significantly aligned" means the motor–DRN angle is significantly smaller than the random baseline (gray), and "significantly orthogonal" for sound–DRN means the angle is significantly closer to 90° than the random baseline.

S3A). We quantified trial-to-trial similarity of sound-evoked subspace activity using cosine similarity, which compares the angle between population activity vectors rather than their magnitude.

Values closer to 1 indicate more similar activity patterns across trials. Interestingly, DRN activation preserved the structure of the auditory population code (Fig. 4E, Fig. S3B). Because head-fixed larvae rarely enter natural sleep, we applied 1 mM mepyramine, a sleep-promoting antihistamine, to induce a sleep-like state (41), which markedly changed auditory responses (Fig. 4E, Fig. S3C). Using both strong and weak auditory stimuli (Fig. S3D), we found no evidence that DRN 5-HT activation altered sound-evoked responses at either intensity (Fig. S3E). Compared against a null distribution – the expected principal angle between two random activity subspaces – our analysis revealed a statistically significant alignment between DRN activation and motor-related neural subspaces, with the sound-related subspace being nearly orthogonal (Fig. 4F and Methods). Here, alignment refers to the geometric relationship between high-dimensional neural subspaces rather than overlap of individual neurons. Thus, DRN 5-HT neuron activation selectively modulates motor-related activity while preserving auditory encoding, thereby reshaping sensorimotor processing.

DRN 5-HT neuron activation produces bout type–dependent, graded suppression of the motor subspace

We constructed a linear regression model using baseline tail movements to predict neural activity (57). After detecting bouts, we computed each bout's direction and amplitude and classified them into 12 types (Fig. S4). Based on the timing of each bout type, we defined 12 regressors (r_1–r_{12}) with corresponding coefficients (β_1-β_{12}) (Fig. 5A, Methods). Using spontaneous behavioral data and motor-correlated dPC1 weight (Fig. S5A), we identified motor-correlated neurons and quantified their coding selectivity using the coefficient of variation (CV) of their 12 regression coefficients. Some neurons showed similar activity across all bout types, yielding low coefficient variability (Fig. 5B top); whereas others responded selectively to specific bout types – such as those involving larger tail amplitudes and turning angles (for instance, type 12) – and therefore displayed higher variability in regression coefficients (Fig. 5B bottom).

We next applied the linear model to predict neural activity during both control and DRN 5-HT activation periods. Although zebrafish exhibited markedly reduced locomotion during DRN 5-HT activation, some motor-correlated neurons maintained control-like activity levels (Fig. 5C, top). However, the neural activity no longer drove movements, indicating a decoupling between neuronal activity and behavior and reducing the variance in neural activity explained by the linear model. In contrast, other neurons displayed a pronounced reduction in activity during 5-HT activation (Fig. 5C, bottom). Using the differences in neuronal activity between control and DRN 5-HT activation, we mapped the spatial distribution of motor-correlated neurons with distinct modulation patterns (Fig. 5D). Interestingly, neurons least affected by DRN 5-HT activation (light red) had lower variability in their regression coefficients, whereas the most affected neurons (dark red) had higher variability (Fig. 5E, Fig. S4B-D). Together, these results suggest that serotonergic modulation exerts a graded suppression on the motor network, preferentially inhibiting downstream neurons involved in specific motor actions to reduce locomotion.

We next asked how DRN 5-HT activation reshapes the geometry of motor-related population activity. We applied Bayesian multi-dimensional scaling (MDS) to the matrix of pairwise neural correlation distances (58) (Fig. S7A). For each neuron pair (i, j) with Pearson correlation C_{ij}, we defined $D_{ij} = \sqrt{2\,(1 - C_{ij})}$ (Methods) so that perfectly correlated neurons have a distance of 0, uncorrelated neurons have a distance of $\sqrt{2}$, and perfectly anti-correlated neurons have a distance of 2. MDS then finds a low-dimensional arrangement of points that best preserves these distances – nearby points have similar activity, and distant points are dissimilar – yielding a geometric snapshot of the population's functional organization. In the Bayesian framework, the geometry of this space is not fixed *a priori*: it compares candidate embeddings and selects the one that best preserves the distances. We tested both flat Euclidean space and hyperbolic space. Hyperbolic space expands exponentially from any point, so distances near its boundary grow much faster

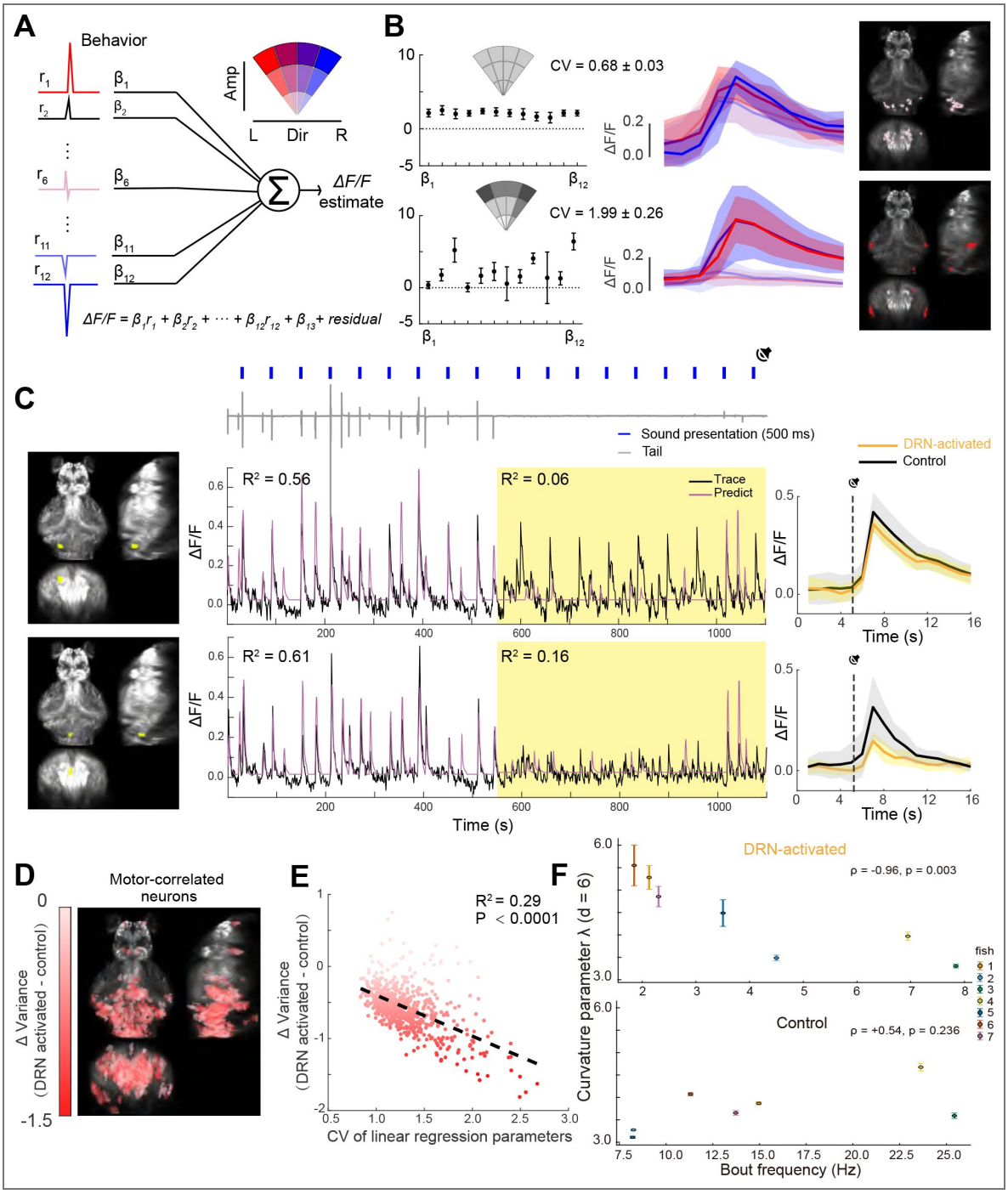

Figure 5. DRN 5-HT neuron activation exerts graded suppression on motor subspace.

A. Schematic of the linear regression analysis. **B**. Example neurons with low (top) and high (bottom) variability in regression coefficients. Left, middle, and right panels show regression coefficients, mean activity across bout types, and neuronal spatial locations. **C**. Two motor-related regions with distinct modulation after DRN 5-HT activation. Left, middle, and right panels show their spatial locations, activity in control and optogenetic trials, and trial-averaged activity. **D**. Spatial distribution of motor-correlated neurons differentially modulated by DRN 5-HT activation. Neural magnitude is quantified by variance. Neurons are color-coded by variance reduction (darker red, stronger suppression; lighter red, weaker effect), as in (Fig. 5E,F). **E**. Relationship between DRN 5-HT–induced modulation and the coefficient of variation (CV) of regression coefficients across motor-correlated neurons. **F**. Hyperbolic curvature of the motor population tracks behavioral quiescence during DRN 5-HT activation. Each point is one fish (n = 7), colored by individual. Y-axis: curvature parameter λ from Bayesian hyperbolic MDS of pairwise motor-population correlation distances ($d = 6$; $K = \lambda^2$); error bars, 1 SD. X-axis: bout frequency in the same period. Top, optogenetic laser on: stronger behavioral suppression corresponds to higher curvature (Spearman $\rho = 0.96$, $p = 0.003$, exact permutation test; Pearson $r = 0.87$, $p = 0.011$). Bottom, laser off: no significant relationship in baseline ($\rho = +0.54$, $p = 0.236$, Pearson $r = +0.59$, $p = 0.166$).

than in a Euclidean space of the same dimension (Fig. S6), making it well suited to data with a hierarchical structure (59, 60), or, more generally, to data in which subsets of points become strongly separated from the rest.

For each fish, we fitted separate embeddings for DRN activation (laser on) and baseline (laser off). The optimal embedding dimension d was between 6 and 8 (Bayesian Information Criterion, see Methods). Hyperbolic embeddings outperformed Euclidean ones in both conditions (Fig. S7C), with curvature parameters λ and $K = -\lambda^2$ ranging from 3.3 to 5.6 across animals and experimental conditions. To test whether the hyperbolic fit captures a meaningful geometrical structure beyond the correlation spectrum, we randomized the eigenvectors (PCA weights) of the covariance matrix while preserving its eigenvalues (Methods). This surrogate still admitted a hyperbolic fit with large λ, but the fit showed systematic distortions: large embedding distances were compressed, deviating from the original distances (Fig. S9A). Thus, the quality of the hyperbolic embedding – its ability to preserve pairwise distances – depends on the specific neuronal arrangement in correlation space.

To further test whether this geometric measure reflects a behavior-dependent reorganization of the motor population rather than the idiosyncrasy of a single recording, we compared the fitted curvature to behavior across animals (Methods). For each fish, we used bout frequency during DRN activation as a readout of how strongly the network was driven toward quiescence (lower frequency = stronger suppression). Across fish (n = 7), laser-on curvature at a given embedding dimension closely tracked this measure (Fig. 5F, Fig. S8): fish in which DRN stimulation nearly abolished swimming showed the highest curvatures, whereas fish with weaker suppression showed lower curvatures (Spearman $\rho = -0.96$, $p = 0.003$, exact permutation test). This coupling was specific to the activated state: during baseline in the same animals, curvature did not significantly relate to spontaneous bout frequency ($\rho = +0.54$, $p = 0.236$), and the trend reversed. Thus, motor-population embedding curvature is a state-dependent geometric signature that appears specifically when DRN 5-HT activation drives the network into quiescence, linking a single population-level parameter to a behavioral phenotype.

Discussion

Activation of DRN 5-HT neurons generally suppresses locomotion in zebrafish, a phenomenon controversially interpreted as sleep or vigilance (18, 44). In this study, DRN 5-HT activation nearly abolished locomotion without altering body posture, and nighttime stimulation still produced normal sleep rebound. Thus, the induced quiescent state represents motor suppression rather than sleep. Unlike mammals, whose sleep states are determined through electroencephalogram (EEG) and electromyogram (EMG) recordings, zebrafish sleep is typically inferred based on several minutes of sustained immobility due to technical limitations (18, 36, 40). Since movement inhibition diminishes responsiveness to external stimuli, this resting yet awake state may be misclassified as sleep in zebrafish.

Indeed, multiple non-sleep behavioral states can also produce pronounced locomotor suppression; previous studies have demonstrated that serotonin contributes to movement suppression across diverse behavioral contexts (44, 46, 48, 49, 52, 61). In our study, zebrafish exhibited spontaneous alternations between locomotor and quiescent states, resembling the previously described “exploitation” and “exploration” modes (46). However, because no prey were present in our experiments, the observed locomotor reduction cannot be equated with the exploitation state. Elevated DRN serotonergic activity has been reported during both REM-like sleep (52) and quiet vigilance (44), and the latter is also associated with low-frequency synchronized forebrain activity (44). A common feature in these distinct states is the pronounced reduction in movement. We therefore propose that DRN serotonergic activation is not sufficient to define a specific behavioral state but primarily drives motor suppression. Consistent with this view, although DRN 5-HT activation strongly suppressed locomotion, we did not observe similar low-frequency synchronized forebrain dynamics during stimulation.

Single-cell connectivity analyses have shown that DRN 5-HT neurons project directly to midbrain and hindbrain regions involved in motor control (62). Consistent with this anatomical organization, whole-brain serotonin imaging has revealed elevated 5-HT levels in the hindbrain during states of reduced motor vigor, where inhibitory HTR1 receptors are predominant (49). At the circuit level, recent voltage imaging studies demonstrate that serotonergic neurons are dynamically regulated by local inhibitory inputs. Swim commands recruit GABAergic inhibition onto DRN 5-HT neurons, leading to a transient reduction in their activity during movement execution (50).

This serotonin-driven motor suppression function appears evolutionarily conserved. In *C. elegans*, activation of serotonergic neurons NSM induces robust locomotor suppression through specific receptor subtypes (10, 15). In mammals, although the serotonergic system has traditionally been regarded as part of the arousal-promoting network, numerous studies have also reported that elevated 5-HT levels suppress locomotion (9, 63–66). This kind of wakeful quiescent state serves important physiological functions. During intense or prolonged physical activity, serotonin levels in the brain and spinal cord rise, inhibiting motor neuron activity and inducing central fatigue, thereby reducing movement to prevent muscle and other bodily damage (67, 68). In a recent study, sick mice activated IL-1R1–expressing serotonergic neurons in the DRN via cytokine signaling, which in turn triggered social withdrawal and reduced locomotion—responses that promote recovery and limit pathogen transmission (66).

In our study, activating DRN 5-HT neurons did not significantly alter the representation of auditory information. The effects on other senses, such as vision or nociception, may differ, and the animal's state could also modify how 5-HT influences sensory encoding. Previous research has observed 5-HT enhancing sensory information encoding under specific conditions (44, 45). In addition, previous studies have shown that under high-threat or punishment-based behavioral paradigms in mice (13), activation of DRN 5-HT neurons can instead increase locomotor activity. Consistently, the environmental threat level may also modulate the effects of DRN serotonergic activity on locomotion in zebrafish.

Finally, our analysis revealed that DRN 5-HT activation does not uniformly inhibit the motor network but instead exerts graded suppression. Neurons with broad tuning across multiple bout types remained largely unaffected, whereas those selectively responsive to specific motor patterns — particularly high-amplitude or turning movements — were strongly suppressed. We also show that the correlation structure of the motor population is well captured in a hyperbolic space, whose curvature serves as a geometric marker of quiescence. These results suggest that serotonergic modulation acts hierarchically at multiple levels of the motor circuitry, preferentially dampening specialized components that drive vigorous or directional movements. Such selective suppression may serve as a mechanism to reduce overall motor output while maintaining baseline motor tone, thereby facilitating rapid transitions between active and quiescent states. This implies that "no-action" is not merely the absence of movement but a strategic policy that prioritizes future state accessibility over immediate output (69), thereby creating the low-noise 'offline' environment (70) essential for learning, neural replay, and memory consolidation.

Methods

Zebrafish

All larval zebrafish were raised in 0.5 × E2 Embryo Media at 28.5°C and a 14/10 hr light/dark cycle. The 0.5 × E2 Embryo Media consists of 7.5 mM NaCl, 0.25 mM KCl, 0.5 mM $MgSO_4$, 75 μM KH_2PO_4, 25 μM Na_2HPO_4, 0.5 mM $CaCl_2$, 0.35 mM $NaHCO_3$. Larval zebrafish aged 6-11 days post-fertilization (dpf) were used for all experiments. Sex discrimination was not included since the sex of zebrafish is not specified at this stage.

All-optical system

Neural activity and behavior were recorded using a custom-built all-optical system, as previously described (51). The system consists of three main components: a 3D tracking module, a dual-color fluorescence imaging module, and an optogenetic manipulation module. A convolutional neural network (CNN) was used to detect the lateral positions of the fish's head from dark-field images captured by the near-infrared (NIR) tracking camera. A tracking model converted the real-time positional information into analog signals to drive the high-speed motorized stage and compensate for fish movement. An autofocus camera with a microlens array acquired multi-perspective images; the fish's z-position was estimated via light-field principles, and a PID controller used this data to drive a piezo for axial tracking. The neural activity-dependent green fluorescence signal and the activity-independent red fluorescence signal were split into two beams by a dichroic mirror before entering the two sCMOS cameras separately. Both the red and green fluorophores can be excited by a blue laser (488 nm). A 2D galvo system deflected a yellow laser (588 nm) to a user-defined ROI in the fish brain for real-time optogenetic manipulation with the aid of a fast whole-brain image reconstruction and registration algorithm.

Experimental procedures for whole-brain imaging and optogenetic manipulation

For freely swimming zebrafish, we employed a custom-designed circular chamber with a diameter of 20 mm and a height of 800 μm. The top and bottom surfaces of the chamber were coverslips, ensuring unobstructed optical access from both above and below. To prevent the chamber edges from occluding fluorescent signals, a 1.5% low-melting-point agarose solution (Thermo Fisher Scientific, product no. 16520050) was used to form an approximately 1 mm wide annular agarose ring around the chamber perimeter. For zebrafish not expressing optogenetic proteins ChrimsonR, the 488 nm laser was operated at 30 mW with a 10 Hz flashing mode and an exposure time of 1 ms per pulse. For zebrafish expressing optogenetic proteins, a long-exposure mode with a reduced power of 0.3 mW was applied to minimize potential interference with the ChrimsonR.

For head-fixed zebrafish, 1.5% low-melting-point agarose was used for immobilization. After the agarose had fully solidified, the agarose surrounding the head (for pharmacological experiments) and tail was carefully removed. Because head fixation substantially reduces motion-induced noise, we used a lower-power 488 nm excitation (0.03 mW) to further minimize interference with the optogenetic proteins ChrimsonR.

In the all-optical system, we incorporated a high-precision patterned optogenetic stimulation module that allowed selective activation of 5-HT neurons within the DRN in both freely swimming and head-fixed zebrafish. The stimulation pattern was spatially restricted to user-defined regions and avoided illumination of the pineal gland. Optogenetic activation was performed using a 588 nm yellow laser. A ROI (160 × 160μm) was positioned to fully encompass the DRN. The laser power was 30 μW, and Galvo-based scanning produced an effective stimulation frequency of 50 Hz. Each optogenetic trial lasted 5 min, with 2–4 repetitions per fish. For experiments that included auditory stimulation, the duration of optogenetic activation was extended as needed to ensure sufficient trial numbers.

Whole-brain image processing pipeline

Whole-brain neural activity was extracted from reconstructed 3D image stacks acquired by the all-optical system. Because both channels originate from the same optical path, spatial transformations are equivalent; registration was therefore first performed on the red channel, which is unaffected by neural activity, and the resulting transformation was applied to the green channel.

Registration included cropping, rigid registration, and non-rigid registration. Reconstructed 3D images (600 × 600 × 250 voxels) were rotated to a standard orientation based on head orientation and cropped to 308 × 380 × 210 voxels to match the ZBB standard brain template. A sharp reference frame without motion blur was selected; all other frames were aligned to this reference

and subsequently registered to the standard brain using affine transformations from the Computational Morphology Toolkit (CMTK, NIH). After rigid registration, small deformations caused by physiological movements were corrected using Demons-based diffeomorphic non-rigid registration. To improve alignment accuracy, an averaged template was generated from 10 frames per 100 frame sequence, and each frame was aligned to this template using optical flow-based registration.

After applying the transformation from the red channel to the green channel, brain regions were segmented based on voxel-wise temporal correlations of the green channel fluorescence. For each voxel, the average correlation with its 14 neighboring voxels was computed to generate a correlation map. The map was segmented using a watershed algorithm to define preliminary regions, and voxels with low correlation to the regional mean were removed. The resulting segmentation was then applied to the red channel.

Behavioral recording and sleep analysis

The experiment began at 18:00 on Day 1 and continued until 12:00 on Day 3, covering two dark cycles. To avoid edge obstruction during imaging, zebrafish larvae were housed in a custom-designed 24 well plate. The light/dark cycle was maintained using white LED illumination (lights on at 08:00 and off at 22:00). A 940 nm infrared light source was used for video recording. Optogenetic stimulation was delivered using a 530 nm LED light source (THORLABS M530L3) during the first 6 hours of the second dark phase. At 14:00 on Day 2, E2 embryo medium and live paramecia were added to prevent dehydration and starvation. Infrared videos were acquired at 1 fps using a Basler acA2000-165kmNIR camera. Illumination control and data acquisition were managed by a custom-written C++ program.

Videos were analyzed using ZebraZoom (*https://zebrazoom.org/*) to extract the locomotor activity of zebrafish larvae. Periods during which swimming speed remained below 0.0667 mm/s (corresponding to 1 pixel in the video, to avoid detection error) for at least 60 s were defined as a quiescent minute. To exclude abnormal data, episodes of continuous immobility lasting longer than 1 hour were removed. The average swimming speed and total immobility duration during the last 4 hours of the first dark phase were then calculated and compared with those from the last 4 hours of the second dark phase to assess the effects of optogenetic stimulation on locomotor activity and sleep-related behavior.

Body roll angle

Zebrafish larvae were approximated as rigid bodies; therefore, the whole brain roll angle was used to estimate the body roll angle. Three-dimensional whole-brain fluorescence data were used for this calculation. Because only the roll angle was required and details of neural activity were not considered, images were downsampled from 2048 × 2048 to 512 × 512 pixels to accelerate processing, followed by deconvolution with 10 iterations. After reconstruction, the 3D images were binarized using adaptive thresholding, and the largest connected component was identified as the head region. Volumes with the largest connected component smaller than 100,000 voxels were considered to correspond to cases in which the fish deviated from the field of view; these data were excluded and filled by interpolation. Principal component analysis (PCA) was applied to determine its principal axis, representing the longitudinal axis of the brain. The brain was then rotated to align this axis with that of a standard reference brain. After alignment, a maximum intensity projection of the 3D image onto the Y–Z plane was generated, and PCA was applied to this projection to determine its principal axis. The angle between this axis and the horizontal vector is defined as the body roll angle of the zebrafish.

At 6 dpf, zebrafish reared under a normal light–dark cycle were subjected to continuous sleep deprivation for 3 days (41). Larvae were placed in a circular tank containing 200 mL of 0.5× E2 embryo medium. The tank was mounted on a shaker and oscillated around its central axis at a frequency of 1 Hz to prevent the larvae from entering a sleep state. Continuous light exposure was

provided throughout the 24 h deprivation period. Paramecia were supplied twice daily to prevent starvation. The medium was replaced daily to maintain optimal water quality. All experiments were conducted during the dark phase (22:00 or later).

Auditory stimuli

Auditory stimuli were integrated into the all-optical system. Binaural sound stimuli (350 Hz, 500 ms duration, 100 dB intensity) were delivered at 60 s intervals. The experimental protocol consisted of an initial baseline period of 10–20 minutes to determine the baseline locomotor speed of each zebrafish, followed by approximately 1 hour of auditory stimulation. During the auditory stimulation period, optogenetic activation was applied using a 588 nm laser in multiple epochs, each lasting 5–10 minutes, with an inter-stimulation interval of at least 10 minutes. Zebrafish behavior was recorded at 50 fps using an infrared camera (Basler acA2000-165kmNIR), and locomotor speed was calculated from the tracked positional data.

For drug-treatment experiments, the protocol consisted of four sequential phases. First, a 20-minute baseline period was recorded. This was followed by a 30-minute auditory stimulation. Subsequently, all E2 embryo medium was removed and replaced with E2 medium containing 1 mM mepyramine. After a 30-minute incubation period to allow the drug to take effect, auditory stimulation was applied again for an additional 30 minutes.

In freely swimming zebrafish, an escape response was defined as an increase in swimming speed exceeding 50% of the baseline average within 1 s following stimulus onset. In head-fixed zebrafish, a DeepLabCut model was trained to detect six key points along the tail to extract locomotor kinematics. Bouts were identified based on the cumulative tail curvature over 0.5 s sliding window, after removing slow trends using a moving average filter with a 9 s window. Bouts occurring within 1 s of auditory stimulus onset were considered stimulus-evoked.

dPCA

dPCA was performed using the MATLAB implementation provided by the Machens laboratory (*https://github.com/machenslab/dPCA*). Head fixation ensured stable whole-brain recording and reliable dimensionality reduction. Prior to analysis, whole-brain neural activity traces were z-score normalized across time. To reduce the influence of sampling noise and motion artifacts, brain regions with volumes smaller than 50 voxels were excluded.

For the identification of the DRN 5-HT activation–related neural subspace, all data were first registered to the standard brain, after which the DRN region itself was removed to prevent direct optogenetic activation effects from dominating the observed activity differences. Neural activity was segmented into trials based on the presence or absence of optogenetic stimulation, without regard to the behavioral state of the fish or the presence of auditory stimuli. Each trial had a fixed duration of 11 s. dPCA was then applied to these trial-structured data. After applying dPCA, we found that in *Tg(tph2:ChrimsonR)* zebrafish, the first demixed principal component (dPC1) explained more than 50% of the total variance, whereas the remaining dPCs accounted for substantially smaller proportions. Therefore, all subsequent analyses were based on dPC1, which was defined as the DRN activation–related subspace. For visualization, dPC1 score for each fish was normalized by its maximum score value and the traces were aligned to DRN optogenetic stimulation onset. Brain regions with high absolute weights on dPC1 were selected, and their spatial distributions were visualized. A linear regression model was used to quantify the fraction of variance in these regions that could be explained by motor behavior (R^2; Methods). To assess the specificity of this relationship, an equal number of neurons was randomly sampled from the remaining whole-brain population (excluding previously removed regions), and their R^2 values were calculated and statistically compared with those of the dPC1-weighted regions.

To identify sound-evoked and motor-correlated neural subspaces, neural activity was categorized into four trial types according to the presence or absence of auditory stimulation and locomotor behavior. Trials containing optogenetic stimulation were excluded from this analysis to avoid confounding effects. Neural activity was temporally aligned either to the onset of auditory stimuli or to the initiation of locomotor bouts. dPCA was then applied using auditory stimulation or

movement as the decoding variable to extract sound-related and motor-related neural components. Because the first demixed principal components (dPC1-sound and dPC1-motor) consistently accounted for a substantially larger fraction of the variance than higher-order components, whole-brain activity was projected onto these components.

Similarity analysis

To quantify the similarity of population neural responses in the sound-evoked subspace across trials under different optogenetic and drug-induced conditions, we constructed trial-by-trial similarity matrices using cosine similarity. Neural activity was z-score normalized across time for each neuron prior to analysis. Trials were defined as the time of auditory stimulus onset and the following 2 s. For each trial, neural activity within the corresponding time window was extracted. Activity for each neuron was then averaged over time to obtain a neurons × 1 vector representing the population response. Population response vectors from all trials were concatenated to form a neurons × trials matrix. Pairwise similarity between trials was computed using cosine similarity across neurons.

Subspace angle analysis

To assess the alignment between the DRN activation–related neural subspace and either the motor-related or sound-evoked subspaces, we quantified subspace similarity using principal angles. For each subspace, the first two dimensions were retained to define the corresponding low-dimensional representation. Orthonormal bases for the DRN activation, motor-related, and sound-evoked subspaces were obtained using the MATLAB function `orth`. Principal angles between each subspace and the DRN activation subspace were then computed using the `subspace` function.

To evaluate the statistical significance of the observed subspace alignment, we performed a nonparametric permutation test. To generate a null distribution, 1,000 random subspaces were constructed by randomly selecting time points from the spontaneous neural activity matrix and orthonormalizing the resulting activity vectors using `orth`. For each random subspace, principal angles relative to the DRN activation subspace were computed using the same procedure, yielding a null distribution of mean principal angles under the hypothesis of random alignment. The observed mean principal angle between the DRN subspace and either the motor-related or sound-related subspace was then compared against the null distribution. Two-tailed empirical p-values were calculated as the proportion of permuted means that were equal to or more extreme than the observed value.

Linear regression

We constructed a linear regression model based on kinematic features extracted from tail motion to quantify how tail movements explain whole-brain neural activity in larval zebrafish. Swimming direction and distance were derived from tail movements, with distance defined as the area swept by the tail during a bout and direction defined as the cumulative tail bending angle within a single bout. Based on these two parameters, a polar coordinate system was constructed, and swimming bouts were classified into 12 discrete types.

For each bout type, a corresponding binary regressor was generated, which took a value of 1 during the occurrence of that bout and 0 otherwise. Each regressor was then convolved with the experimentally measured jGCaMP8s calcium response kernel. The resulting regressors formed the matrix X. For each neuron, the linear regression model was defined as

$$y(t) = \beta_0 + \sum_{i=1}^{12} \beta_i X_i(t) + \varepsilon(t)$$

where $y(t)$ denotes the neural activity time series, $X_i(t)$ represents the convolved regressor for the i-th bout type, β_i is the corresponding regression coefficient, β_0 is the intercept, and $\varepsilon(t)$ denotes the residual error.

Model fitting was performed using the MATLAB function `fitlm` with ordinary least squares estimation. The coefficient of determination (R^2) was calculated for each neuron to quantify the proportion of variance in neural activity explained by motor behavior.

For each fish, to avoid confounding effects, only tail movement data recorded during the baseline period without optogenetic stimulation or auditory stimulation were used to construct the model. Fish whose baseline tail movements were insufficient to cover all 12 bout types were excluded from further analysis. Motor-related neurons were then identified based on both the proportion of variance in neural activity explained by movement (R^2) and their weights in the motor-related subspace. To quantify the effect of optogenetic stimulation on motor-related neurons, the model fitted during the baseline period was used to predict their neural activity during both the control (no stimulation) and DRN 5-HT activation periods.

Hyperbolic and Euclidean Multidimensional Scaling

We analyzed the geometry of motor population activity using multidimensional scaling (MDS) on pairwise neural correlation distance matrices. Pairwise distances between motor-correlated neurons were computed from the Pearson correlation matrix C as

$$D_{ij} = \sqrt{2\,(1 - C_{ij})}$$

This is the chord distance on the unit hypersphere of z-scored activity vectors and is a proper metric ($D_{ij} = D_{ji}$, $D_{ii} = 0$, triangle inequality satisfied), which is required for the validity of the Bayesian MDS embedding and the Bayesian Information Criterion (BIC) based dimensionality selection. Distances are bounded in [0, 2], with $D_{ij} = 0$ for perfectly correlated, $D_{ij} = \sqrt{2}$ for uncorrelated, and $D_{ij} = 2$ for perfectly anticorrelated neurons.

Our main analysis used Bayesian hyperbolic MDS (HMDS) to embed the data in a Poincaré ball, following Praturu et al. (58). Using the `metric_HMDS` Python library, we jointly optimized the embedded coordinates and a global curvature parameter λ (constant negative curvature $K = -\lambda^2$) so that hyperbolic distances δ_{ij} best matched the neural distances D_{ij}:

$$D_{ij} = \frac{\delta_{ij}}{\lambda} + \epsilon_{ij}$$

The embedding dimension ($d = 6$) was chosen by minimizing the Bayesian Information Criterion (BIC) over candidate dimensions, defined as

$$\mathrm{BIC} = k \ln(n) - 2 \ln(\hat{L})$$

where $\hat{L}$ is the maximized model likelihood, k is the number of free parameters, and n is the number of observations. For a distance matrix of N points, $n = N\,(N - 1)/2$. For the HMDS model with embedding dimension d, the effective number of parameters is

$$k_{\mathrm{HMDS}} = Nd + 1 + N - \frac{d(d-1)}{2}$$

accounting for N points in d dimensions, one global curvature λ, N point-specific uncertainty parameters, and adjusting for the rotational symmetry of hyperbolic space. We found the optimal embedding d by minimizing BIC (Fig. S7B). For comparison, we applied classical Euclidean MDS (`scikit-learn, dissimilarity='precomputed', metric=True`) with the same dimension. Its BIC used $N \times d$ coordinate parameters and one global variance parameter.

To estimate intrinsic variability in pairwise neural correlation distances from non-stationary brain dynamics, we performed a time-window–based uncertainty analysis. Each recording was divided into non-overlapping 60 s windows. For each window, we computed population activity vectors and the corresponding pairwise correlation distance matrix. We then calculated, for each unique pair, the variance of its distance across windows, yielding a distribution of temporal stability. This produced a variance matrix Σ_D with the same dimensions as the averaged distance matrix D, where $\Sigma_D(i, j)$ is the empirical temporal variance of the distance between neurons i and j. These variance estimates were incorporated into both HMDS and Euclidean MDS by weighting each pairwise distance in the likelihood function inversely by its variance.

We visualized the embeddings to interpret the geometry. For dimensions > 3, we projected the coordinates into 3D using PCA and displayed them within the Poincaré ball. Embedding quality was evaluated with Shepard diagrams (Fig. S7C), plotting original distances against embedded distances. A perfect embedding would place all points on the $y = x$ diagonal.

Eigenvector-randomization surrogate

To test whether the fitted hyperbolic curvature reflects genuine geometric structure in the motor population rather than spectral properties of the shared variance alone, we generated surrogate datasets that preserve the eigenvalue spectrum of the covariance matrix while destroying the arrangement of which neurons participate in which mode.Specifically, we computed the covariance matrix Σ of the activity traces across motor-correlated neurons and eigendecomposed it as $\Sigma = U \Lambda U^{\top}$. We then replaced the eigenvector matrix U with a random orthonormal basis U', drawn uniformly from $O(N)$ via QR decomposition of a random Gaussian matrix, and reconstructed a surrogate covariance matrix $\Sigma' = U' \Lambda U'^{\top}$. The surrogate covariance was converted to a correlation matrix $C'_{ij} = \frac{\Sigma'_{ij}}{\sqrt{\Sigma'_{ii}\Sigma'_{jj}}}$ from which pairwise distances were computed. We applied the full HMDS pipeline to C' under identical settings and compared the fitted curvature λ and the Shepard diagram to those from the original data (Fig. S9B).

Cross-animal analysis of curvature and behavior

For each fish, we computed bout frequency separately for laser-on and laser-off periods as swim bouts per second. Bouts were detected from the tracked tail trace using the cumulative tail-curvature criterion described above (“Bout detection”). Each correlation distance matrix was normalized by a scaling factor such that the maximum distance D_{ij} was equal to 2. Curvature was fit independently for each fish and condition using the HMDS procedure above. To obtain an estimate of fit uncertainty for λ, we repeated the HMDS optimization multiple times per fish and per condition from different random initializations. The reported λ values are mean ± SD across these repeats. Fit uncertainty was systematically larger during DRN activation than during baseline, consistent with a more strongly warped embedding being harder for the optimizer to localize precisely. We quantified associations between bout frequency and fitted curvature λ with Spearman rank correlation ρ, and obtained two-sided p-values by exact permutation: for each comparison, we evaluated all 7! = 5040 permutations of λ across fish, computed ρ for each, and took the fraction with $|\rho_{\text{perm}}| \geq |\rho_{\text{observed}}|$ as the exact p-value. This avoids the asymptotic assumptions of the standard Spearman test, which are unreliable at $n = 7$. Pearson correlations and their parametric p-values are reported for comparison.

Statistical analysis

Wilcoxon matched-pairs signed rank test and Mann–Whitney U test were used and data are expressed as the mean ± min-max in Fig. 2C. Mann–Whitney U test was used in Fig. 1D. Mann–Whitney U test was used and data are expressed as the mean ± min-max in Fig. 2D and Fig. 3D. Wilcoxon matched-pairs signed rank test was used in Fig. 4B. P-values obtained via a nonparametric permutation test in Fig. 4F. Data are expressed as the mean ± SD in Fig. 1D, Fig. 2B, Fig. 5B, Fig. 5C.

Data availability

The Bayesian multi-dimensional scaling (MDS) code in this work can be found at *https://github.com/wenquan/BayesianHMDS*. The figure plotting code can be found at *https://github.com/kexin2016/zebrafish-quiescent-state*. The fish data collected and analyzed in this work can be found at *https://doi.org/10.6084/m9.figshare.32121937* Raw imaging data are available upon request from the corresponding author.

Supplementary figures

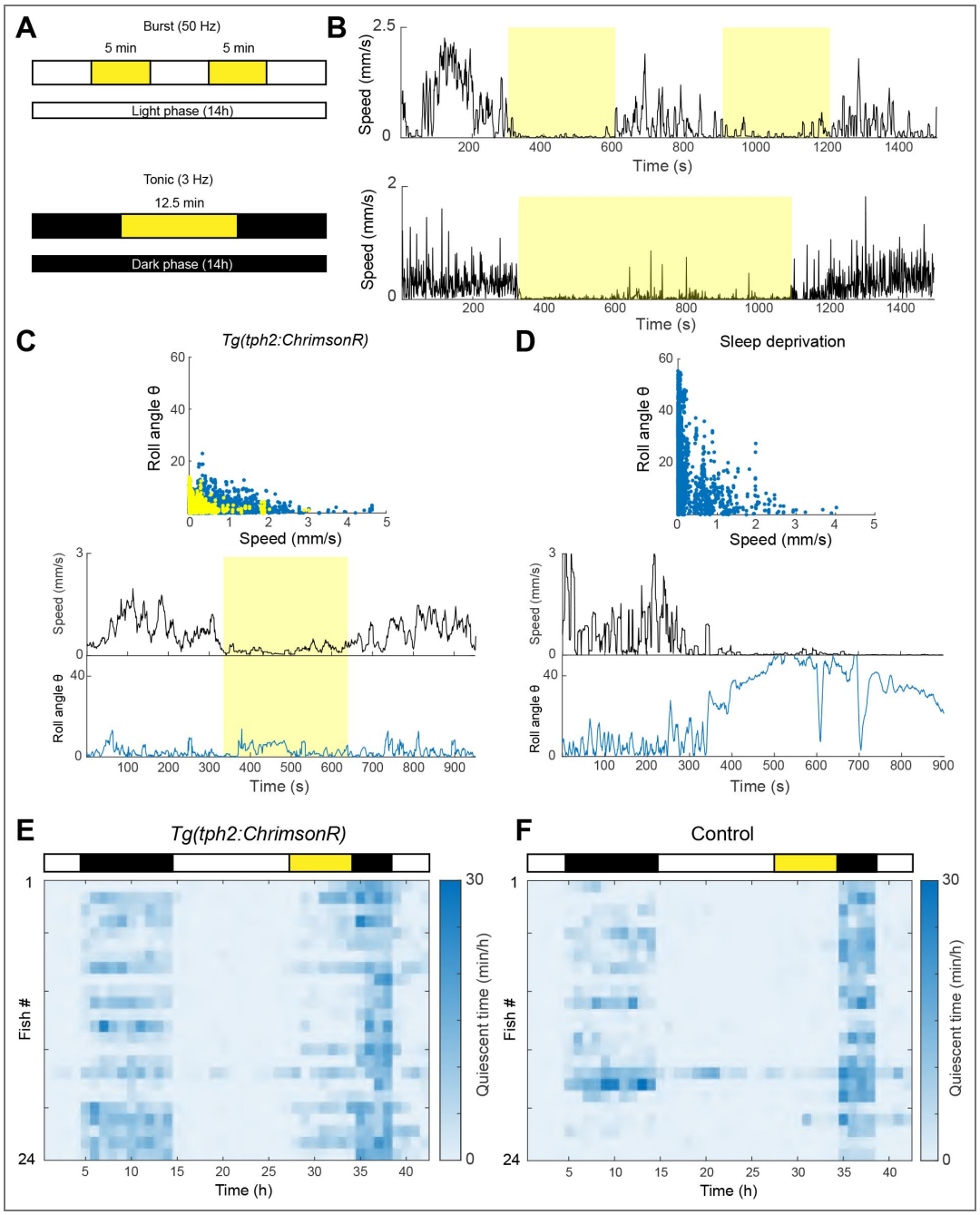

Figure S1. DRN 5-HT activation suppresses locomotion and induces a quiescent state distinct from sleep. A. Schematic of burst and tonic optogenetic stimulation paradigms. **B**. Top: locomotor speed of a zebrafish during burst stimulation. Bottom: locomotor speed of a zebrafish during tonic stimulation. **C**. Relationship between body roll angle and swimming speed in Tph2:ChrimsonR zebrafish. Each point represents one second; yellow points indicate periods of DRN 5-HT activation. **D**. Relationship between body roll angle and swimming speed in sleep-deprived zebrafish. **E**. Quiescence per hour in Tph2:ChrimsonR zebrafish. **F**. Quiescence per hour in control zebrafish.

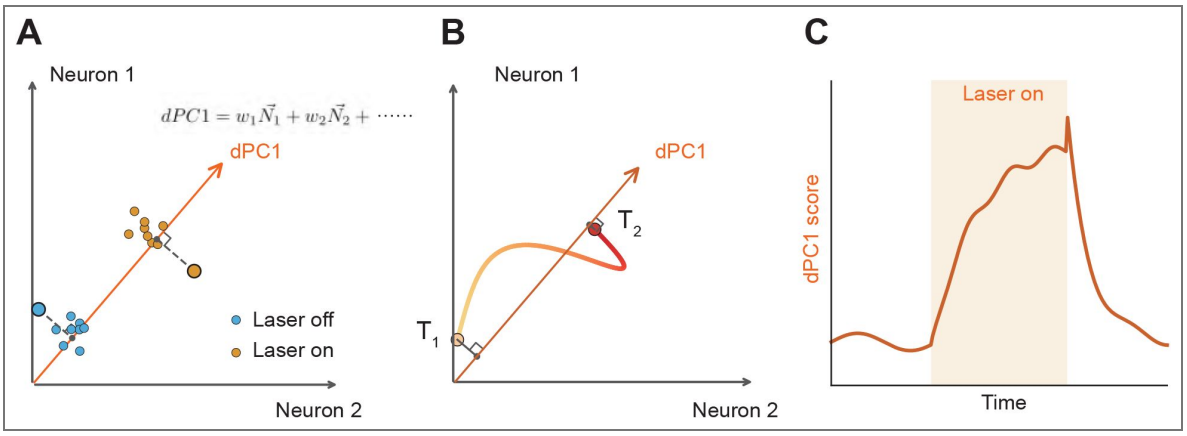

Figure S2. Geometric interpretation of dPCA.

A. Neural activity at each time point is a point in an N-dimensional space defined by the recorded neurons (illustrated for two neurons). dPCA finds a direction (dPC1, orange arrow) that best separates conditions — here, DRN-activated (orange) versus control (blue). Dashed lines show orthogonal projections of individual time points onto the dPC1 axis. The weights defining dPC1 as a linear combination of the neural axes are shown below. **B**. Over time, the population state traces a trajectory through this space (color gradient from light to dark indicates progression from T_1 to T_2). Projecting this trajectory onto dPC1 (dashed lines with right-angle marks) gives a one-dimensional time course of the activation-related component of population activity. **C**. The resulting dPC1 score, plotted as a time series with the laser-on period shaded, is the quantity shown in Fig. 3B and reflects how strongly the population is driven along the activation-related direction at each moment.

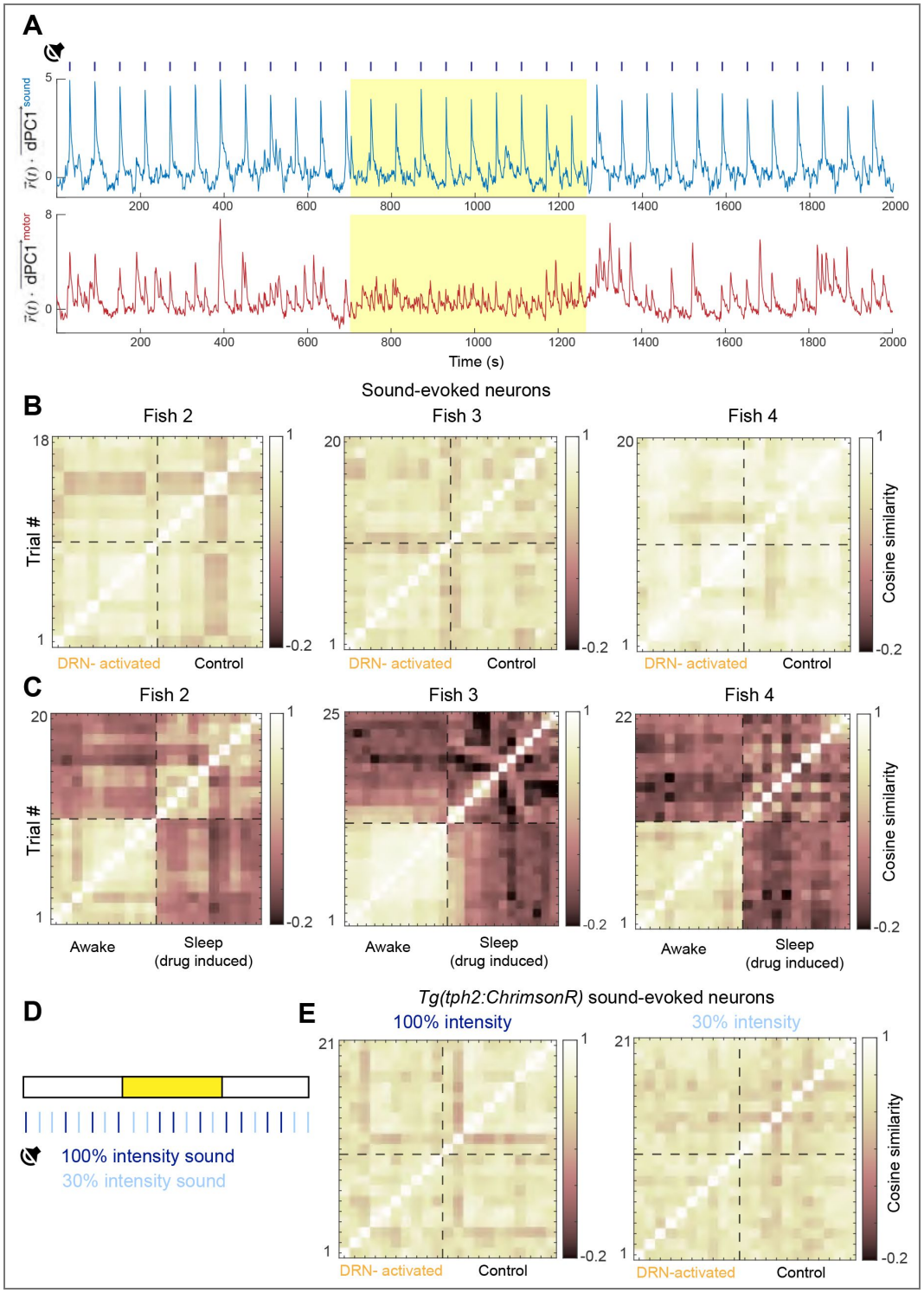

Figure S3. DRN 5-HT activation did not alter neural dynamics within the sound-evoked subspace.

A. Temporal evolution of whole-brain neural activity projected onto the sound-evoked subspace and the motor-correlated subspace in an example Tg(tph2:ChrimsonR) zebrafish. Yellow shading indicates periods of optogenetic stimulation. **B**. Similarity matrices of sound-evoked neuronal population responses during DRN 5-HT activation and control periods for fish 2–4 (fish 1 shown in Fig. 4E). **C**. Same analysis as in panel B, but comparing the awake state with the drug-induced sleep state. **D**. Schematic of auditory stimulation paradigms with different sound intensities. **E**. Similarity matrices of sound-evoked neuronal population responses for strong (left) and weak (right) sound stimuli during DRN 5-HT activation and control periods.

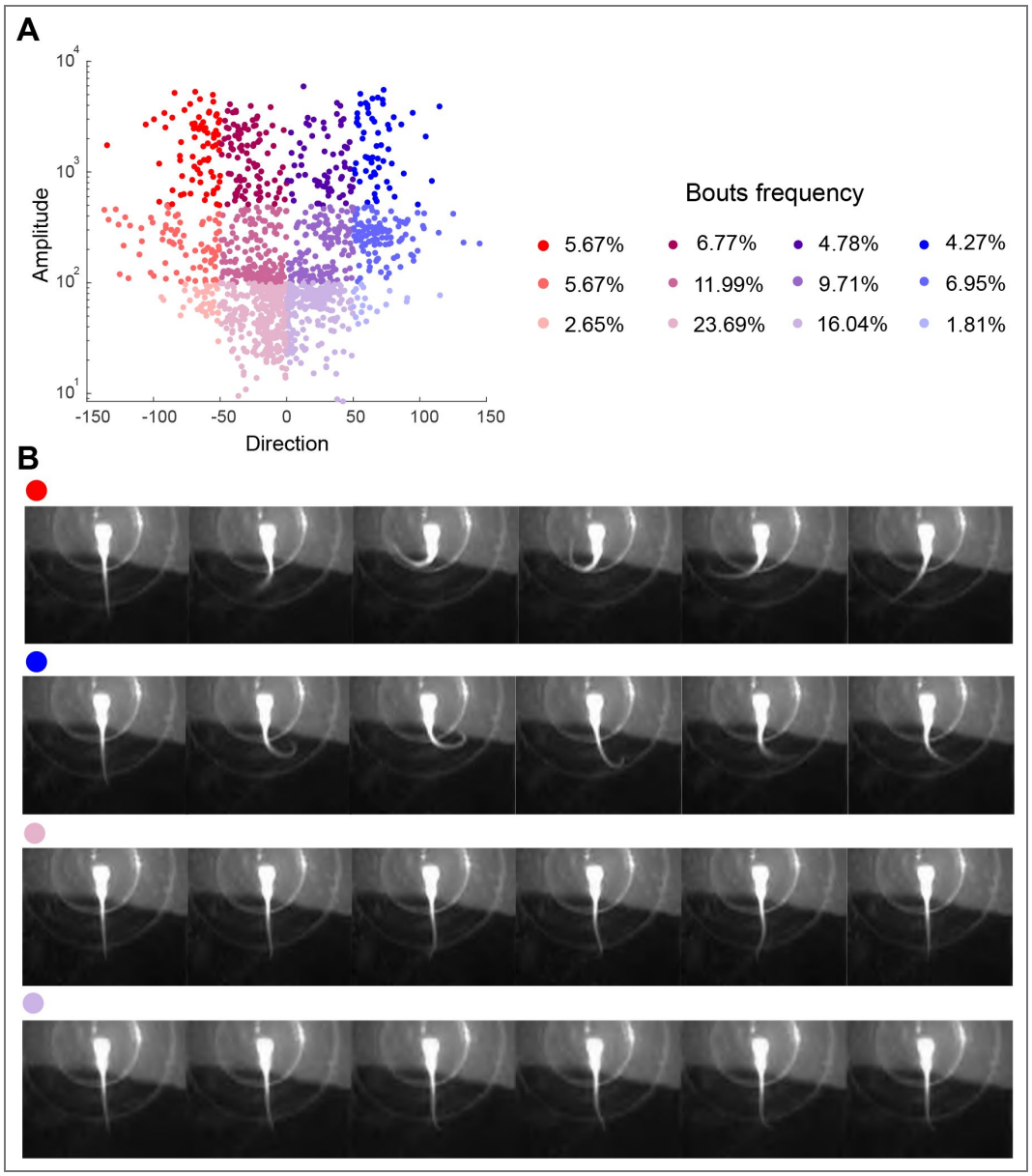

Figure S4. Distribution of bouts in the direction–amplitude space.

A.Left: Distribution of all detected bouts projected onto the direction–amplitude space. Each bout is color-coded according to the classification scheme used in the main text (n = 7 fish, 1,493 bouts). Right: Frequency distribution of each bout type. **B**. Representative examples of distinct bout types, illustrating both large- and small-amplitude tail deflections. Colors are consistent with those used in the main figures.

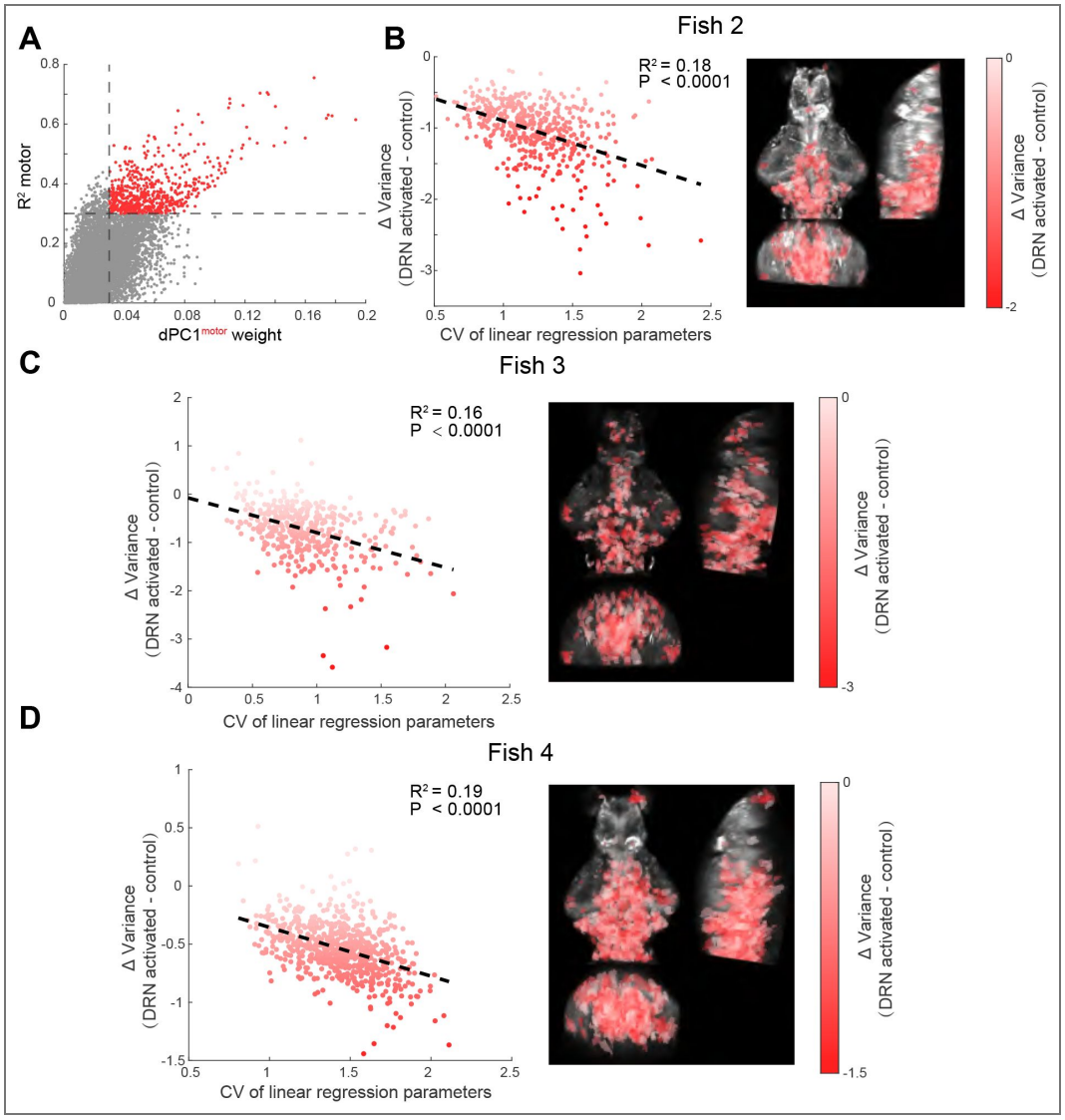

Figure S5. DRN 5-HT activation exerts graded suppression on the motor subspace.

A. Relationship between *dP C1*^{motor} weights and R^2. Red points indicate the motor-correlated neurons included in the analysis. **B-D**. Relationship between DRN 5-HT activation–induced modulation of neural activity and the coefficient of variation (CV) of regression coefficients in motor-correlated neurons for fish 2–4 (fish 1 shown in Fig. 5D–E).

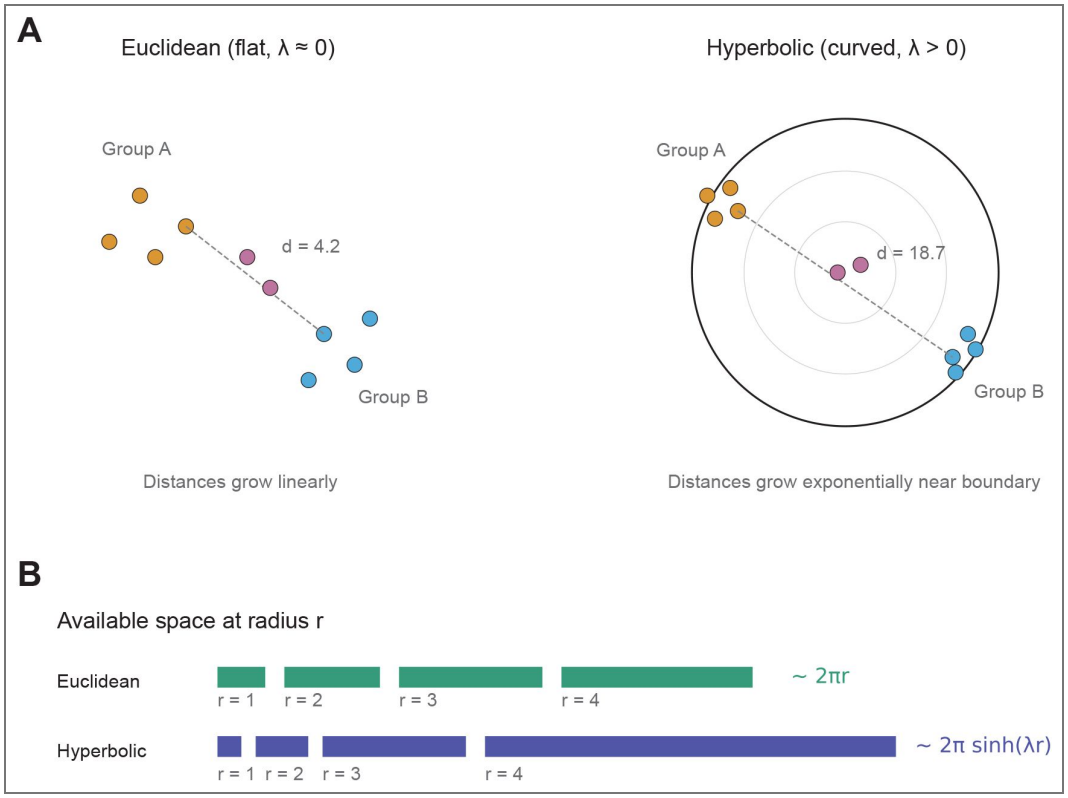

Figure S6. Intuition for hyperbolic versus Euclidean embedding.

The same neuron population (colored by functional group) embedded in flat Euclidean space (left) and in a Poincaré disk representation of hyperbolic space (right). In Euclidean geometry, distances between groups grow linearly, so separation is moderate. In hyperbolic geometry, space near the disk boundary expands exponentially, allowing functionally distinct groups (orange, blue) to be far more separated than in an equally dimensional Euclidean space, even though they appear visually close in the disk. Dashed lines show the distance between the same two groups in each geometry. Pink points near the center lie at moderate distance from both groups. Bottom inset: available space (circumference) at radius r grows as $\sim 2\pi r$ in Euclidean geometry but as $\sim 2\pi \sinh \lambda r$ in hyperbolic geometry, where λ is the curvature parameter. This exponential expansion lets hyperbolic embeddings accommodate populations with strongly segregated functional subsets.

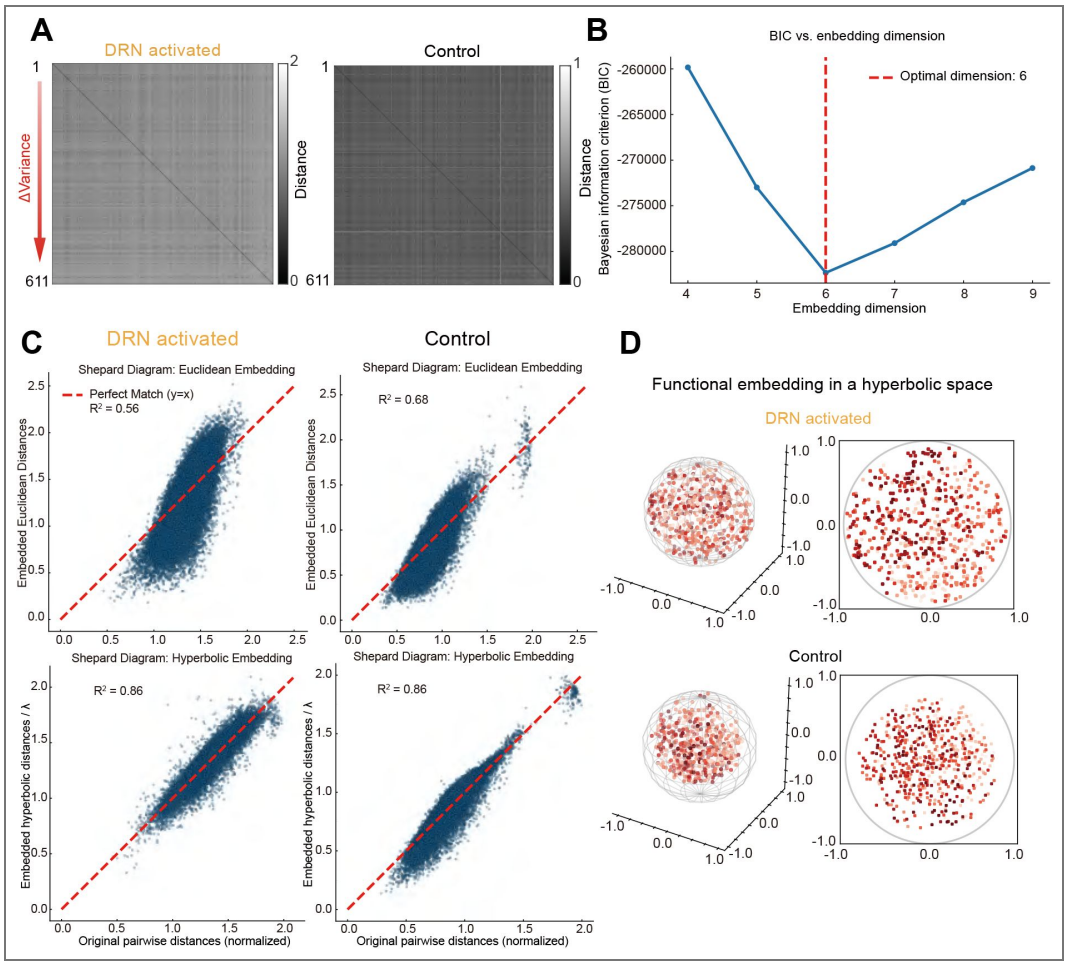

Figure S7. DRN 5-HT activation diversifies motor network activity.

A. Pairwise distance matrices of motor-correlated neurons during DRN activation (left) and control (right) periods (fish 1). Neural activity magnitude was quantified by the variance. Neurons were ranked by changes in variance between DRN 5-HT activation and control periods. **B**. Embedding dimension as a function of BIC, see Methods. **C**. Shepard diagram of embedded vs. original pairwise distances for fish 1. Original distance matrices were scaled so the maximum distance is 2. Left: DRN activation (laser on); Right: baseline (laser off). Top: Euclidean embedding; bottom: hyperbolic embedding. As indicated by R^2, hyperbolic embedding outperforms Euclidean embedding under all conditions, consistently across all fish. Embedding dimension $d = 6$. **D**. Hyperbolic multidimensional scaling (HMDS) of neural correlation distances in a 3D Poincaré ball (left) and 2D projection (right), see Methods. Top: functional embedding during DRN 5-HT activation; bottom: control. In the Poincaré ball, distances diverge near the boundary. During DRN activation, two neuronal ensembles segregated to opposite poles (light and dark red, as in Fig. 5E), indicating increased functional diversity, whereas at baseline the embedding was more compact.

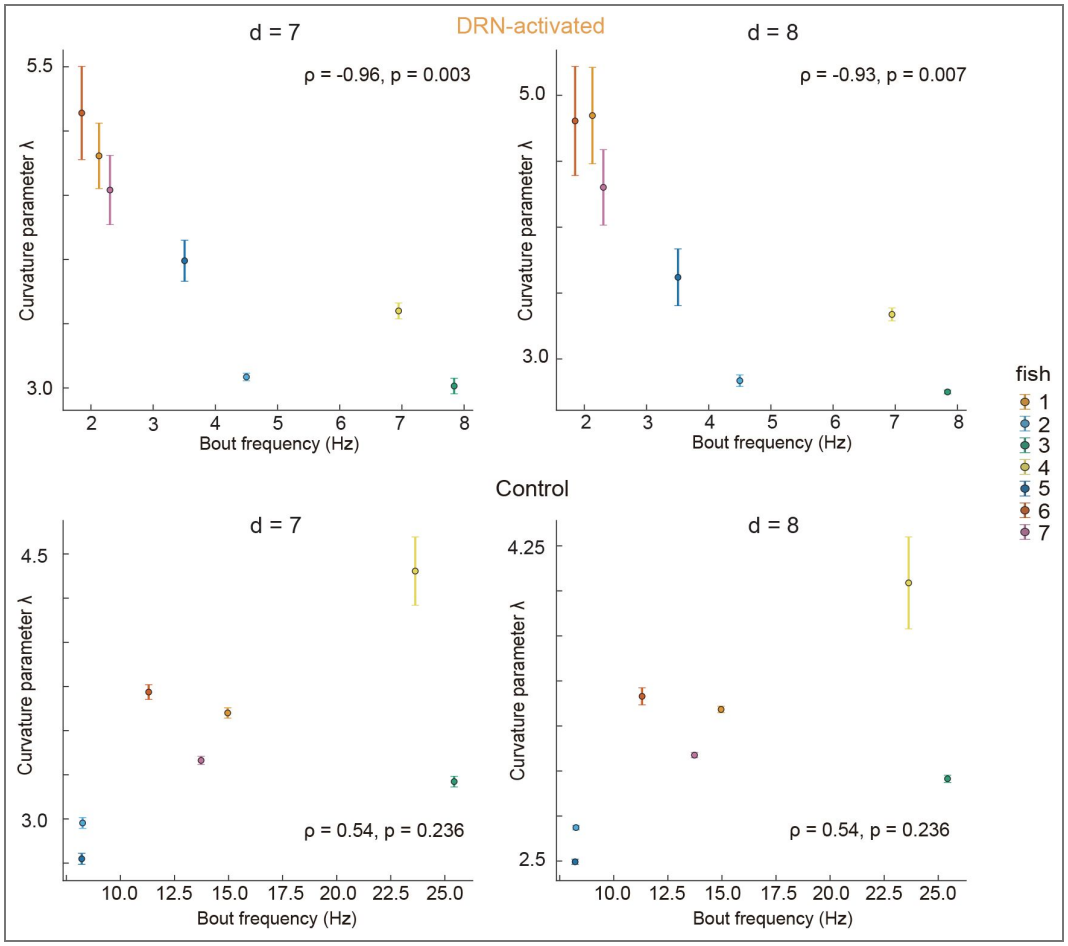

Figure S8. Curvature–behavior relationship is robust across embedding dimensions.

Same analysis as Fig. 5F but with embedding dimensions d = 7 (left column) and d = 8 (right column). Top row: during DRN activation, λ correlates negatively with bout frequency at both d = 7 (Spearman ρ = 0.96, p = 0.003) and d = 8 (Spearman ρ = 0.93, p = 0.007, exact permutation tests). Bottom row: no significant relationship during baseline in either dimension. Each point is one zebrafish (n = 7), colored by individual; error bars, ± 1 SD from the HMDS fit. All p-values computed by exact permutation (5040 permutations).

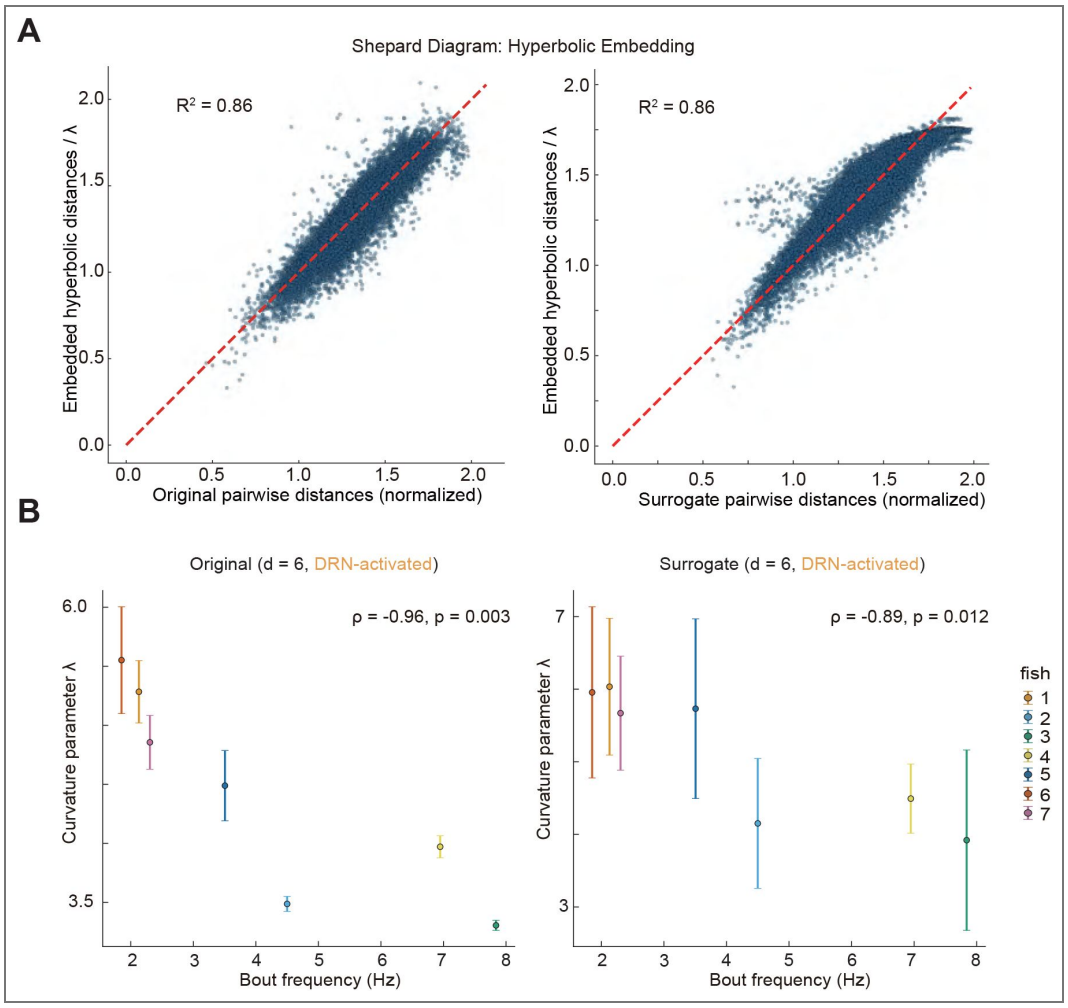

Figure S9. Eigenvector-randomized surrogate distorts pairwise correlation distances.

A. Shepard diagrams for hyperbolic embedding of original (left) and surrogate data (right). Left, original motor-population data (fish 1) during DRN activation. Points track the diagonal with approximately symmetric scatter. Right, covariance-eigenvector-randomized surrogate. The surrogate was generated by replacing the eigenvectors of the covariance matrix with a random orthonormal basis while preserving the eigenvalue spectrum (Methods). The cloud systematically deviates below the diagonal at large distances, indicating that the surrogate embedding compresses distances between dissimilar neurons. This distortion is absent in the original data, confirming that the quality of the hyperbolic fit depends on the specific geometric arrangement of neurons in correlation space, not solely on the eigenvalue spectrum of the covariance matrix. Shepard diagrams for other fish exhibit qualitatively similar behaviors. **B**. Curvature parameter λ vs. laser-on bout frequency for original data (left) and surrogate data (right), both at d = 6. Each point is one zebrafish (n = 7); error bars, ± 1 SD across repeated HMDS fits. The surrogate yields substantially larger fit uncertainty, indicating that the optimizer cannot converge on a stable embedding in the absence of a specific geometric structure. The tight curvature–behavior correlation observed in the original data is also weakened in the surrogate.

Acknowledgements

The authors are grateful to Danqian Liu for experimental suggestions, Yu Mu for sharing the optogenetic fish line, Takashi Kawashima for sharing unpublished datasets, and Rubén Moreno Bote for discussions. This research was supported by the STI2030–Major Projects (Grant No. 2022ZD0211900), under the subproject “New Technologies for Whole-Brain-Scale Neuronal Mesoscopic Atlas” (Grant No. 2022ZD0211904).

Additional information

Funding

Funder	Grant reference number	Author
STI2030-Major Projects	2022ZD0211900	Guodong Tan Quan Wen Kexin Qi Yuming Chai Daguang Li

Author ORCID iDs

Yuming Chai: https://orcid.org/0000-0003-0184-1824
Quan Wen: https://orcid.org/0000-0003-0268-8403

References

1. **Descarries L.,** Alain B., Watkins K. C. (1975) Serotonin nerve terminals in adult rat neocortex. *Brain research* **100**:563-588 https://doi.org/10.1016/0006-8993(75)90158-4 | PubMed
2. **Jacobs B. L.,** Azmitia E. C. (1992) Structure and function of the brain serotonin system. *Physiological reviews* **72**:165-229 https://doi.org/10.1152/physrev.1992.72.1.165 | PubMed
3. **Dayan P.,** Huys Q. J. (2009) Serotonin in affective control. *Annual review of neuroscience* **32**:95-126 https://doi.org/10.1146/annurev.neuro.051508.135607 | PubMed
4. **Lee S.-H.,** Dan Y. (2012) Neuromodulation of brain states. *neuron* **76**:209-222 https://doi.org/10.1016/j.neuron.2012.09.012 | PubMed
5. **Hamada H. T.,** Abe Y., Takata N., Taira M., Tanaka K. F., Doya K. (2024) Optogenetic activation of dorsal raphe serotonin neurons induces brain-wide activation. *Nature communications* **15**:4152 https://doi.org/10.1038/s41467-024-48489-6 | PubMed
6. **Meijer G. T.,** Catarino J. A., Freitas-Silva L., Laranjeira I., Laboratory I. B., Mainen Z. F. (2025) Serotonin drives choice-independent reconfiguration of distributed neural activity. *bioRxiv* 2025.08.01.668048 https://doi.org/10.1101/2025.08.01.668048
7. **Jacobs B. L.,** Fornal C. A. (1993) 5-ht and motor control: a hypothesis. *Trends in neurosciences* **16**:346-352 https://doi.org/10.1016/0166-2236(93)90090-9 | PubMed
8. **Brustein E.,** Chong M., Holmqvist B., Drapeau P. (2003) Serotonin patterns locomotor network activity in the developing zebrafish by modulating quiescent periods. *Journal of neurobiology* **57**:303-322 https://doi.org/10.1002/neu.10292 | PubMed
9. **Correia P. A.,** Lottem E., Banerjee D., Machado A. S., Carey M. R., Mainen Z. F. (2017) Transient inhibition and long-term facilitation of locomotion by phasic optogenetic activation of serotonin neurons. *eLife* **6**:e20975 https://doi.org/10.7554/eLife.20975 | PubMed
10. **Flavell S. W.,** Pokala N., Macosko E. Z., Albrecht D. R., Larsch J., Bargmann C. I. (2013) Serotonin and the neuropeptide pdf initiate and extend opposing behavioral states in c. elegans. *Cell* **154**:1023-1035 https://doi.org/10.1016/j.cell.2013.08.001 | PubMed

11. **Montgomery J. E.,** Wahlstrom-Helgren S., Wiggin T. D., Corwin B. M., Lillesaar C., Masino M. A. (2018) Intraspinal serotonergic signaling suppresses locomotor activity in larval zebrafish. *Developmental Neurobiology* **78**:807-827 https://doi.org/10.1002/dneu.22606 | PubMed

12. **Perrier J.-F.,** Rasmussen H. B., Jørgensen L. K., Berg R. W. (2018) Intense activity of the raphe spinal pathway depresses motor activity via a serotonin dependent mechanism. *Frontiers in Neural Circuits* **11**:111 https://doi.org/10.3389/fncir.2017.00111 | PubMed

13. **Seo C.,** Guru A., Jin M., Ito B., Sleezer B. J., Ho Y.-Y., Wang E., Boada C., Krupa N. A., Kullakanda D. S., *et al.* (2019) Intense threat switches dorsal raphe serotonin neurons to a paradoxical operational mode. *Science* **363**:538-542 https://doi.org/10.1126/science.aau8722 | PubMed

14. **Andalman A. S.,** Burns V. M., Lovett-Barron M., Broxton M., Poole B., Yang S. J., Grosenick L., Lerner T. N., Chen R., Benster T., *et al.* (2019) Neuronal dynamics regulating brain and behavioral state transitions. *Cell* **177**:970-985 https://doi.org/10.1016/j.cell.2019.02.037 | PubMed

15. **Dag U.,** Nwabudike I., Kang D., Gomes M. A., Kim J., Atanas A. A., Bueno E., Estrem C., Pugliese S., Wang Z., *et al.* (2023) Dissecting the functional organization of the c. elegans serotonergic system at whole-brain scale. *Cell* **186**:2574-2592 https://doi.org/10.1016/j.cell.2023.04.023 | PubMed

16. **Jouvet M.** (1969) Biogenic amines and the states of sleep: Pharmacological and neurophysiological studies suggest a relationship between brain serotonin and sleep. *Science* **163**:32-41 https://doi.org/10.1126/science.163.3862.32 | PubMed

17. **McGinty D. J.,** Harper R. M. (1976) Dorsal raphe neurons: depression of firing during sleep in cats. *Brain research* **101**:569-575 https://doi.org/10.1016/0006-8993(76)90480-7 | PubMed

18. **Oikonomou G.,** Altermatt M., Zhang R.-w., Coughlin G. M., Montz C., Gradinaru V., Prober D. A. (2019) The serotonergic raphe promote sleep in zebrafish and mice. *Neuron* **103**:686-701 https://doi.org/10.1016/j.neuron.2019.05.038 | PubMed

19. **Venner A.,** Broadhurst R. Y., Sohn L. T., Todd W. D., Fuller P. M. (2020) Selective activation of serotoninergic dorsal raphe neurons facilitates sleep through anxiolysis. *Sleep* **43**:zsz231 https://doi.org/10.1093/sleep/zsz231 | PubMed

20. **Lee D. A.,** Oikonomou G., Cammidge T., Andreev A., Hong Y., Hurley H., Prober D. A. (2020) Neuropeptide vf neurons promote sleep via the serotonergic raphe. *eLife* **9**:e54491 https://doi.org/10.7554/eLife.54491 | PubMed

21. **Cools R.,** Roberts A. C., Robbins T. W. (2008) Serotoninergic regulation of emotional and behavioural control processes. *Trends in cognitive sciences* **12**:31-40 https://doi.org/10.1016/j.tics.2007.10.011 | PubMed

22. **Marcinkiewcz C. A.,** Mazzone C. M., D'Agostino G., Halladay L. R., Hardaway J. A., DiBerto J. F., Navarro M., Burnham N., Cristiano C., Dorrier C. E., *et al.* (2016) Serotonin engages an anxiety and fear-promoting circuit in the extended amygdala. *Nature* **537**:97-101 https://doi.org/10.1038/nature19318 | PubMed

23. **Braun D.,** Rosenberg A. M., Rabaniam E., Haruvi R., Malamud D., Barbara R., Aiznkot T., Levavi-Sivan B., Kawashima T. (2024) High-resolution tracking of unconfined zebrafish behavior reveals stimulatory and anxiolytic effects of psilocybin. *Molecular Psychiatry* **29**:1046-1062 https://doi.org/10.1038/s41380-023-02391-7 | PubMed

24. **Cohen J. Y.,** Amoroso M. W., Uchida N. (2015) Serotonergic neurons signal reward and punishment on multiple timescales. *eLife* **4**:e06346 https://doi.org/10.7554/eLife.06346 | PubMed

25. **Li Y.,** Zhong W., Wang D., Feng Q., Liu Z., Zhou J., Jia C., Hu F., Zeng J., Guo Q., *et al.* (2016) Serotonin neurons in the dorsal raphe nucleus encode reward signals. *Nature communications* **7**:10503 https://doi.org/10.1038/ncomms10503 | PubMed

26. **Matias S.,** Lottem E., Dugué G. P., Mainen Z. F. (2017) Activity patterns of serotonin neurons underlying cognitive flexibility. *eLife* **6**:e20552 https://doi.org/10.7554/eLife.20552 | PubMed

27. **Iigaya K.,** Fonseca M. S., Murakami M., Mainen Z. F., Dayan P. (2018) An effect of serotonergic stimulation on learning rates for rewards apparent after long intertrial intervals. *Nature communications* **9**:2477 https://doi.org/10.1038/s41467-018-04840-2 | PubMed

28. **Grossman C. D.,** Bari B. A., Cohen J. Y. (2022) Serotonin neurons modulate learning rate through uncertainty. *Current Biology* **32**:586-599 https://doi.org/10.1016/j.cub.2021.12.006 | PubMed

29. **Azmitia E. C.,** Segal M. (1978) An autoradiographic analysis of the differential ascending projections of the dorsal and median raphe nuclei in the rat. *Journal of comparative neurology* **179**:641-667 https://doi.org/10.1002/cne.901790311 | PubMed

30. **Scammell T. E.,** Arrigoni E., Lipton J. O. (2017) Neural circuitry of wakefulness and sleep. *Neuron* **93**:747-765 https://doi.org/10.1016/j.neuron.2017.01.014 | PubMed

31. **Wang Y.,** Wang D., Zhang X., Li H., Wang S., He Y., Zhao G., Dong H., Li J. (2024) Dorsal raphe serotonergic neurons-ventral tegmental area neural pathway promotes wake from sleep. *CNS Neuroscience & Therapeutics* **30**:e70141 https://doi.org/10.1111/cns.70141 | PubMed

32. **Jouvet M.** (1968) Insomnia and decrease of cerebral 5-hydroxytryptamine after destruction of the raphe system in the cat. *Advances in pharmacology* **6**:265-279 https://doi.org/10.1016/s1054-3589(08)60326-9 | PubMed

33. **Portas C. M.,** Bjorvatn B., Ursin R. (2000) Serotonin and the sleep/wake cycle: special emphasis on microdialysis studies. *Progress in neurobiology* **60**:13-35 https://doi.org/10.1016/s0301-0082(98)00097-5 | PubMed

34. **Monti J. M.** (2011) Serotonin control of sleep-wake behavior. *Sleep medicine reviews* **15**:269-281 https://doi.org/10.1016/j.smrv.2010.11.003 | PubMed

35. **Zhdanova I. V.,** Wang S. Y., Leclair O. U., Danilova N. P. (2001) Melatonin promotes sleep-like state in zebrafish. *Brain research* **903**:263-268 https://doi.org/10.1016/s0006-8993(01)02444-1 | PubMed

36. **Prober D. A.,** Rihel J., Onah A. A., Sung R.-J., Schier A. F. (2006) Hypocretin/orexin overexpression induces an insomnia-like phenotype in zebrafish. *Journal of Neuroscience* **26**:13400-13410 https://doi.org/10.1523/jneurosci.4332-06.2006 | PubMed

37. **Yokogawa T.,** Marin W., Faraco J., Pézeron G., Appelbaum L., Zhang J., Rosa F., Mourrain P., Mignot E. (2007) Characterization of sleep in zebrafish and insomnia in hypocretin receptor mutants. *PLoS biology* **5**:e277 https://doi.org/10.1371/journal.pbio.0050277 | PubMed

38. **Rihel J.,** Prober D. A., Arvanites A., Lam K., Zimmerman S., Jang S., Haggarty S. J., Kokel D., Rubin L. L., Peterson R. T., *et al.* (2010) Zebrafish behavioral profiling links drugs to biological targets and rest/wake regulation. *Science* **327**:348-351 https://doi.org/10.1126/science.1183090 | PubMed

39. **Oikonomou G.,** Prober D. A. (2017) Attacking sleep from a new angle: contributions from zebrafish. *Current opinion in neurobiology* **44**:80-88 https://doi.org/10.1016/j.conb.2017.03.009 | PubMed

40. **Lee D. A.,** Andreev A., Truong T. V., Chen A., Hill A. J., Oikonomou G., Pham U., Hong Y. K., Tran S., Glass L., *et al.* (2017) Genetic and neuronal regulation of sleep by neuropeptide vf. *eLife* **6**:e25727 https://doi.org/10.7554/eLife.25727 | PubMed

41. **Leung L. C.,** Wang G. X., Madelaine R., Skariah G., Kawakami K., Deisseroth K., Urban A. E., Mourrain P. (2019) Neural signatures of sleep in zebrafish. *Nature* **571**:198-204 https://doi.org/10.1038/s41586-019-1336-7 | PubMed

42. **Lillesaar C.** (2011) The serotonergic system in fish. *Journal of chemical neuroanatomy* **41**:294-308 https://doi.org/10.1016/j.jchemneu.2011.05.009 | PubMed

43. **Lovett-Barron M.,** Andalman A. S., Allen W. E., Vesuna S., Kauvar I., Burns V. M., Deisseroth K. (2017) Ancestral circuits for the coordinated modulation of brain state. *Cell* **171**:1411-1423 https://doi.org/10.1016/j.cell.2017.10.021 | PubMed

44. **Zhao Y.,** Huang C.-X., Gu Y., Zhao Y., Ren W., Wang Y., Chen J., Guan N. N., Song J. (2024) Serotonergic modulation of vigilance states in zebrafish and mice. *Nature Communications* **15**:2596 https://doi.org/10.1038/s41467-024-47021-0 | PubMed

45. **Yokogawa T.,** Hannan M. C., Burgess H. A. (2012) The dorsal raphe modulates sensory responsiveness during arousal in zebrafish. *Journal of Neuroscience* **32**:15205-15215 https://doi.org/10.1523/jneurosci.1019-12.2012 | PubMed

46. **Marques J. C.,** Li M., Schaak D., Robson D. N., Li J. M. (2020) Internal state dynamics shape brainwide activity and foraging behaviour. *Nature* **577**:239-243 https://doi.org/10.1038/s41586-019-1858-z | PubMed

47. **Ahrens M. B.,** Li J. M., Orger M. B., Robson D. N., Schier A. F., Engert F., Portugues R. (2012) Brain-wide neuronal dynamics during motor adaptation in zebrafish. *Nature* **485**:471-477 https://doi.org/10.1038/nature11057 | PubMed

48. **Kawashima T.,** Zwart M. F., Yang C.-T., Mensh B. D., Ahrens M. B. (2016) The serotonergic system tracks the outcomes of actions to mediate short-term motor learning. *Cell* **167**:933-946 https://doi.org/10.1016/j.cell.2016.09.055 | PubMed

49. **Haruvi R.,** Barbara R., Shainer I., Rosenberg A., Moshe L., Malamud D., Toledano J., Braun D., Baier H., Kawashima T. (2024) Global and compartmentalized serotonergic control of sensorimotor integration underlying motor adaptation. *BioRxiv* 2024.09.15.613094 https://doi.org/10.1101/2024.09.15.613094

50. **Kawashima T.,** Wei Z., Haruvi R., Shainer I., Narayan S., Baier H., Ahrens M. B. (2025) Voltage imaging reveals circuit computations in the raphe underlying serotonin-mediated motor vigor learning. *Neuron* https://doi.org/10.1016/j.neuron.2025.05.017 | PubMed

51. **Chai Y.,** Qi K., Wu Y., Li D., Tan G., Guo Y., Chu J., Mu Y., Shen C., Wen Q. (2024) All-optical interrogation of brain-wide activity in freely swimming larval zebrafish. *Iscience* **27** https://doi.org/10.1016/j.isci.2023.108385 | PubMed

52. **Choudhary V.,** Heller C. R., Aimon S., de Sardenberg Schmid L., Robson D. N., Li J. M. (2023) Neural and behavioral organization of rapid eye movement sleep in zebrafish. *bioRxiv* 2023.08.28.555077 https://doi.org/10.1101/2023.08.28.555077

53. **Kobak D.,** Brendel W., Constantinidis C., Feierstein C. E., Kepecs A., Mainen Z. F., Qi X.-L., Romo R., Uchida N., Machens C. K. (2016) Demixed principal component analysis of neural population data. *eLife* **5**:e10989 https://doi.org/10.7554/eLife.10989 | PubMed

54. **Zada D.,** Appelbaum L. (2020) Chapter 9 - behavioral criteria and techniques to define sleep in zebrafish. In: Gerlai R. T. (Ed). *Behavioral and Neural Genetics of Zebrafish* Academic Press. pp. 141-153 https://doi.org/10.1016/B978-0-12-817528-6.00009-7

55. **Privat M.,** Romano S. A., Pietri T., Jouary A., Boulanger-Weill J., Elbaz N., Duchemin A., Soares D., Sumbre G. (2019) Sensorimotor transformations in the zebrafish auditory system. *Current Biology* **29**:4010-4023.e4, https://doi.org/10.1016/j.cub.2019.10.020 | PubMed

56. **Pantoja C.,** Hoagland A., Carroll E. C., Karalis V., Conner A., Isacoff E. Y. (2016) Neuromodulatory regulation of behavioral individuality in zebrafish. *Neuron* **91**:587-601 https://doi.org/10.1016/j.neuron.2016.06.016 | PubMed

57. **Dunn T. W.,** Mu Y., Narayan S., Randlett O., Naumann E. A., Yang C.-T., Schier A. F., Freeman J., Engert F., Ahrens M. B. (2016) Brain-wide mapping of neural activity controlling zebrafish exploratory locomotion. *eLife* **5**:e12741 https://doi.org/10.7554/eLife.12741 | PubMed

58. **Praturu A.,** Sharpee T. O. (2024) Adaptive data embedding for curved spaces. *Iscience* **27** https://doi.org/10.1016/j.isci.2024.111266 | PubMed

59. **Krioukov D.,** Papadopoulos F., Kitsak M., Vahdat M., Boguñá M. (2010) Hyperbolic geometry of complex networks. *Physical Review E* **82**:036106 https://doi.org/10.1103/PhysRevE.82.036106 | PubMed

60. **Zhou Y.,** Smith B. H., Sharpee T. O. (2018) Hyperbolic geometry of the olfactory space. *Science Advances* **4**:eaq1458 https://doi.org/10.1126/sciadv.aaq1458 | PubMed

61. **Mu Y.,** Bennett D. V., Rubinov M., Narayan S., Yang C.-T., Tanimoto M., Mensh B. D., Looger L. L., Ahrens M. B. (2019) Glia accumulate evidence that actions are futile and suppress unsuccessful behavior. *Cell* **178**:27-43 https://doi.org/10.1016/j.cell.2019.05.050 | PubMed

62. **Song Z.,** Huang C.-X., Zhang H., Ye C., Guan N., Song J. (2025) Integrated single-cell atlases unveil the operation principles of whole-brain 5-ht neuronal subsystems. *Science Advances* **11**:eadv8128 https://doi.org/10.1126/sciadv.adv8128 | PubMed

63. **Green R.,** Gillin J., Wyatt R. (1976) The inhibitory effect of intraventricular administration of serotonin on spontaneous motor activity of rats. *Psychopharmacology* **51**:81-84 https://doi.org/10.1007/bf00426326 | PubMed

64. **Fonseca M. S.,** Murakami M., Mainen Z. F. (2015) Activation of dorsal raphe serotonergic neurons promotes waiting but is not reinforcing. *Current Biology* **25**:306-315 https://doi.org/10.1016/j.cub.2014.12.002 | PubMed

65. **Ren J.,** Friedmann D., Xiong J., Liu C. D., Ferguson B. R., Weerakkody T., DeLoach K. E., Ran C., Pun A., Sun Y., *et al.* (2018) Anatomically defined and functionally distinct dorsal raphe serotonin sub-systems. *Cell* **175**:472-487 https://doi.org/10.1016/j.cell.2018.07.043 | PubMed

66. **Yang L.,** Andina M. L., Witkowski M., King H., Wickersham I., Huh J. R., Choi G. B. (2025) Il-1r1-positive dorsal raphe neurons drive self-imposed social withdrawal in sickness. *Cell* https://doi.org/10.1016/j.cell.2025.10.040 | PubMed

67. **Meeusen R.,** Watson P., Hasegawa H., Roelands B., Piacentini M. F. (2006) Central fatigue: the serotonin hypothesis and beyond. *Sports Medicine* **36**:881-909 https://doi.org/10.2165/00007256-200636100-00006 | PubMed

68. **Cotel F.,** Exley R., Cragg S. J., Perrier J.-F. (2013) Serotonin spillover onto the axon initial segment of motoneurons induces central fatigue by inhibiting action potential initiation. *Proceedings of the National Academy of Sciences* **110**:4774-4779 https://doi.org/10.1073/pnas.1216150110 | PubMed

69. **Ramírez-Ruiz J.,** Grytskyy D., Mastrogiuseppe C., Habib Y., Moreno-Bote R. (2024) Complex behavior from intrinsic motivation to occupy future action-state path space. *Nature Communications* **15**:6368 https://doi.org/10.1038/s41467-024-49711-1 | PubMed

70. **Sutton R. S.,** Barto A. G. (2018) *Reinforcement Learning: An Introduction* (second) Cambridge, MA, USA: MIT Press.

Kexin Qi, Yuming Chai, Guodong Tan, Daguang Li, Quan Wen (2026) Serotonergic modulation of motor subspace dynamics drives a sleep-independent quiescent state. figshare. https://doi.org/10.6084/m9.figshare.32121937

Peer reviews

Reviewer #1 (Public review):

The wide-ranging serotonergic projections emerging from the Dorsal Raphe nucleus (DRN) is suggestive of a central role in regulating brain-wide activity and behavioural states. DRN activity has been associated to diverse functions, ranging from mood, motivation and pain regulation to sleep and cognitive flexibility. Its far-reaching connectivity made it challenging to assess the brain-wide effect of its activation, especially during behaviour.

The present study by Qi et al. addresses these challenges by combining state-of-the-art tracking microscopy with the whole-brain accessibility of the larval zebrafish model. To investigate the effect of DRN activation, the authors leveraged the Tg(tph2:ChrimsonR) line to optogenetically activate tph2-positive neurons in the DRN, while monitoring changes in brain-wide activity, locomotion and auditory-stimuli evoked responses.

Optogenetic activation had a suppressing effect on locomotion, which the authors distinguished from inducing sleep by the maintenance of posture and its sleep disturbing effect of nighttime stimulations. Further, the authors report a distinct effect of DRN activation on motor-related, but not auditory-related neuronal subspaces, identified by demixed principal component analysis.

In addition, rather than affecting all motor-correlated neurons similarly, tph2+ DRN-mediated suppression focused on neurons encoding high-amplitude or turning motion.

In summary, the work of Qi et al. provides solid evidence for a predominant role of the DRN in wake-state motor suppression by aptly combining the vast data-acquisition possibilities of the larval zebrafish model with computational methods to extract relevant information.

The brain-wide scope of the analysis is a key strength, reducing bias, confirming the involvement of known motor and auditory regions, and providing a valuable dataset for future analyses.

While the results well support the conclusion of the authors, certain biological and technical aspects demand discussion.

Comments on revised version.

The authors successfully addressed my points.

https://doi.org/10.7554/eLife.110370.2.sa2

Reviewer #2 (Public review):

Summary:

The authors examine the effects of activating the dorsal raphe nucleus serotonergic system using a combination of calcium imaging and optogenetics in freely moving larval zebrafish. Their findings show that optogenetic stimulation induces a state of behavioral quiescence.

They further investigate whether this state corresponds to sleep or reduced motor activity. Analyses of posture and sleep-related paradigms indicate that serotonergic activation primarily suppresses motor output rather than promoting sleep. Notably, this suppression appears to be bout type-dependent, with stronger effects on neurons associated with larger tail amplitudes and turning angles.

In addition, auditory stimulation experiments reveal no significant impact of serotonin on sound encoding.

Strengths:

The study combines advanced experimental techniques with state-of-the-art analytical methods, enabling precise and compelling insights into the role of serotonergic modulation. The experiments and analyses are well aligned with the questions being addressed, and the results appear robust and reliable.

Moreover, the implementation of experiments that combine calcium imaging and optogenetics in freely moving animals is technically challenging and appears well justified in the context of the research questions.

Weaknesses:

While the authors discuss different quiescent states mediated by serotonin reported in previous studies, more thorough attempt to determine whether the observed state corresponds to any of the previously described forms of quiescence, or represents a subset or variant of them, would strengthen the manuscript. This would help better integrate the findings with the existing literature.

While addressing these questions may require substantial further work, potentially beyond the scope of the present study, the availability of whole-brain data provides an opportunity to

at least explore or discuss these possibilities. In particular, it would be interesting to examine the recruitment of regions not directly stimulated but known to be associated with other neuromodulatory systems or promoting glial activation (e.g., the locus coeruleus).

https://doi.org/10.7554/eLife.110370.2.sa1

Author response:

The following is the authors' response to the original reviews.

In response to the reviewers' comments, we have made revisions to the manuscript. Specifically, we have:

(1) Increased the sample size in the whole-brain imaging and demixed principal component analysis (dPCA) analyses presented in Figures 1 and 3, strengthening the statistical support for our conclusions;

(2) Revised the presentation of Figure 3B to clarify that the displayed dPC1 traces were scaled for visualization purposes only (dPC1 / max(dPC1)), rather than normalized for quantitative comparison across animals;

(3) Expanded the main text and supplementary figures to provide more intuitive explanations and geometric illustrations of dPCA and hyperbolic space analysis, and clarified the interpretation of correlation matrices and principal-angle analyses to improve readability;

(4) Substantially expanded the sections on Bayesian multidimensional scaling and hyperbolic embedding, including additional methodological details and validation analyses to strengthen the computational framework and its interpretation;

(5) Expanded the Discussion to incorporate recent studies and discuss potential mechanisms underlying DRN 5-HT-mediated motor suppression.

We believe that these revisions have substantially strengthened the manuscript and addressed the major concerns raised during peer review.

> ***Reviewer #1 (Public review):***
>
> *The wide-ranging serotonergic projections emerging from the Dorsal Raphe nucleus (DRN) are suggestive of a central role in regulating brain-wide activity and behavioural states. DRN activity has been associated with diverse functions, ranging from mood, motivation and pain regulation to sleep and cognitive flexibility. Its far-reaching connectivity made it challenging to assess the brain-wide effect of its activation, especially during behaviour.*
>
> *The present study by Qi et al. addresses these challenges by combining state-of-the-art tracking microscopy with the whole-brain accessibility of the larval zebrafish model. To investigate the effect of DRN activation, the authors leveraged the Tg(tph2:ChrimsonR) line to optogenetically activate tph2-positive neurons in the DRN, while monitoring changes in brain-wide activity, locomotion and auditory-stimuli evoked responses.*
>
> *Optogenetic activation had a suppressing effect on locomotion, which the authors distinguished from inducing sleep by the maintenance of posture and its sleep disturbing effect of nighttime stimulations. Further, the authors report a distinct effect of DRN activation on motor-related, but not auditoryrelated neuronal subspaces, identified by demixed principal component analysis.*

> *In addition, rather than affecting all motor-correlated neurons similarly, tph2+ DRN-mediated suppression focused on neurons encoding high-amplitude or turning motion.*
>
> *In summary, the work of Qi et al. provides solid evidence for a predominant role of the DRN in wake-state motor suppression by aptly combining the vast data-acquisition possibilities of the larval zebrafish model with computational methods to extract relevant information.*
>
> *The brain-wide scope of the analysis is a key strength, reducing bias, confirming the involvement of known motor and auditory regions, and providing a valuable dataset for future analyses.*
>
> *While the results well support the conclusion of the authors, certain biological and technical aspects demand discussion.*

We thank you for the positive and thoughtful evaluation of our work. We also appreciate your constructive comments on the biological and technical aspects of the study. We have carefully considered these concerns and addressed them point-by-point below, with corresponding revisions to the manuscript.

> ***Reviewer #1 (Recommendations for the authors):***
>
> *(1) Further samples required:*
>
> *Figure 1D relies on n=3 with lots of variability; the author should add more Ns to illustrate their point (typically 10-15 fish used per study to show reliability across fish).*
>
> *Figure 3 also relies only on 5 fish in each condition; the authors should increase to 10-15 to show variability.*

Thank you for this valuable suggestion. To address this concern, we have increased the sample size in the revised manuscript. Specifically, the number of animals in Figure 1D has been increased from n = 3 to n = 5, and additional statistical analyses have been included to strengthen the quantitative support for our conclusions. Note that the error bars are plotted as standard deviation (SD), which may make the variability appear larger. In Figure 3, the number of animals was also increased from n = 5 to n = 8.

In addition, our findings are consistent with previous work showing a strong association between elevated dorsal raphe nucleus (DRN) activity and reduced locomotion in zebrafish [1, 2, 3]. Importantly, across animals, the variance explained by the dPCA components and the rapid modulation of whole-brain state remain highly consistent, supporting the robustness and reproducibility of our observations.

Given this increased sample size together with consistency across animals and convergence with prior studies, we believe the current dataset provides sufficient statistical and biological support for our conclusions.

> *(2) Further steps to be added to the analysis to fully support the claim:*
>
> *It appears that the individual brains are registered and individually clustered into areas by combining highly-correlated nearby neurons.*
>
> *dPCA is then computed for individual brains. Evidence for our interpretation of individual dPCA spaces:*
>
> *(1) Figure 3A depicts separate dPCs for different fish.*

> *(2) Line 488–489 describes normalization of the value range of dPCs to compare across fish, which implies separate dPCs.*
>
> *While the authors normalize the projections onto the principal components, the dPCA spaces remain individual, as does the meaning of their components. It is thus questionable how to conclude from data across fish in a rigorous manner.*
>
> *Instead, we recommend that the authors build voxels for each individual's brain and calculate dPCA across all brains, not individual ones, so that components could become truly comparable across the brains of given individuals.*

We thank the reviewer for this important comment. We would like to clarify that our analysis does not aim to construct a shared dPCA space across animals or to quantitatively compare dPC scores between individuals. In this analysis, dPCA was performed separately for each fish to capture the dominant low-dimensional population dynamics within each individual brain.

The purpose of Figure 2 is to demonstrate that DRN activation induces a rapid and robust transition in whole-brain activity, rather than to define a common population subspace across animals.

We also attempted to register and pool data across animals for a joint analysis, as suggested by the reviewer. However, our dataset includes zebrafish at slightly different developmental stages (6–12 dpf). Although the behavioral effects of DRN activation (including motor suppression and global brain-state modulation) were robust across this age range, developmental differences introduced substantial anatomical variability in brain size and morphology, which reduced registration accuracy and made voxel-wise correspondence across animals unreliable.

We realize that our previous description of "normalization" may have caused confusion. To clarify, the dPC1 traces shown in Figure 2 were only scaled for visualization by dividing each fish's projection by its maximum value (dPC1 / max(dPC1)), so that trajectories from different fish could be displayed on the same axis. This scaling does not alter the underlying dPCA space, does not constitute normalization for cross-animal comparison, and was not used for any quantitative analysis.

Importantly, despite being computed independently for each fish, we observed a consistent temporal pattern across animals: DRN activation was reliably accompanied by a rapid transition captured by dPC1 in each individual fish. We have revised the Methods and corresponding text in the manuscript to make this distinction explicit and avoid ambiguity.

> ***Reviewer #2 (Public review):***
>
> *Summary:*
>
> *The authors examine the effects of activating the dorsal raphe nucleus serotonergic system using a combination of calcium imaging and optogenetics in freely moving larval zebrafish. Their findings show that optogenetic stimulation induces a state of behavioral quiescence.*
>
> *They further investigate whether this state corresponds to sleep or reduced motor activity. Analyses of posture and sleep-related paradigms indicate that serotonergic activation primarily suppresses motor output rather than promoting sleep. Notably, this suppression appears to be bout type-dependent, with stronger effects on neurons associated with larger tail amplitudes and turning angles.*

> *In addition, auditory stimulation experiments reveal no significant impact of serotonin on sound encoding.*

We thank the reviewer for the careful and thoughtful summary of our work.

> *Strengths:*
>
> *The study combines advanced experimental techniques with state-of-the-art analytical methods, enabling precise and compelling insights into the role of serotonergic modulation. The experiments and analyses are well aligned with the questions being addressed, and the results appear robust and reliable.*
>
> *Moreover, the implementation of experiments that combine calcium imaging and optogenetics in freely moving animals is technically challenging and appears well justified in the context of the research questions.*

We thank you for the positive assessment of our work and for recognizing the technical and analytical strengths of our experimental approach.

We address the reviewer's specific comments in detail below.

> *Weaknesses:*
>
> *While the analytical techniques employed are sophisticated and appear to be appropriately applied, their presentation makes the manuscript difficult to follow. Although the explanations are provided in the Methods section, including more guidance in the main text, such as how to interpret each analytical approach and what outcomes would be expected under different scenarios, would help readers who are less familiar with these techniques.*
>
> *Providing this context would better guide the reader in navigating the figures, broaden the accessibility of the work, and ultimately increase its impact.*

We thank you for this important suggestion. To improve clarity and accessibility, we have revised the main text to provide more intuitive explanations of both demixed principal component analysis (dPCA) and hyperbolic space analysis, with additional emphasis on how to interpret their outputs and what different outcomes imply biologically.

Additionally, we have included new supplementary figures (Figure S2 and Figure S6) with geometric illustrations and simplified examples to provide a more visual and conceptual understanding of these methods. We hope these revisions make the analytical framework easier to follow and improve the accessibility and impact of the manuscript.

> *While the authors discuss different quiescent states mediated by serotonin reported in previous studies, their interpretation is limited to stating that "a common feature shared by these distinct behavioral states is a pronounced reduction in movement," and consequently proposing that activation of dorsal raphe nucleus is not sufficient to specify a particular behavioral state, but rather plays a primary role in driving motor suppression.*
>
> *In my view, a more thorough attempt to determine whether the observed state corresponds to any of the previously described forms of quiescence, or represents a subset or variant of them, would strengthen the manuscript. This would help better integrate the findings with the existing literature.*

> *For example, given that the authors have access to whole-brain activity data, it would be valuable to examine and discuss whether there are shared patterns of activation with previously reported quiescent states.*

Thank you for the insightful suggestion. To address this, we compared our whole-brain activity patterns with key neural signatures reported in previously characterized zebrafish quiescent states.

A recent study reported that exposure to conspecific alarm substance (CAS) induces a quiescent but vigilant state associated with elevated DRN 5-HT activity and low-frequency synchronized forebrain activity [3]. In our dataset, although DRN 5-HT activation similarly induced robust locomotor suppression, we did not detect comparable low-frequency synchronized forebrain dynamics during the stimulation period. These results suggest that while DRN 5-HT activation is sufficient to induce motor suppression, it does not recapitulate the full neural signature of CAS-induced vigilant quiescence. We have incorporated this comparison and its interpretation into the Discussion section of the revised manuscript.

Following the termination of optogenetic stimulation, we observed a gradual recovery of locomotory speed, consistent with the behavior in an earlier study [3], although our recovery was much faster. Interestingly, whole brain imaging also revealed a transient increase in forebrain activity. This elevated forebrain activity gradually returned to baseline as locomotor activity recovered. In accordance with the reviewer's suggestion, we propose that these forebrain dynamics represent a common motif that facilitates the transition out of the DRN-induced quiescent state (Author response image 1.).

> *The manuscript largely avoids discussing the mechanisms underlying the observed motor suppression. For instance, is this effect driven directly by serotonin release onto target neurons? Is it mediated by glial activity, as suggested in other studies? Are additional neuromodulatory systems being recruited?*
>
> *While addressing these questions may require substantial further work, potentially beyond the scope of the present study, the availability of whole-brain data provides an opportunity to at least explore or*

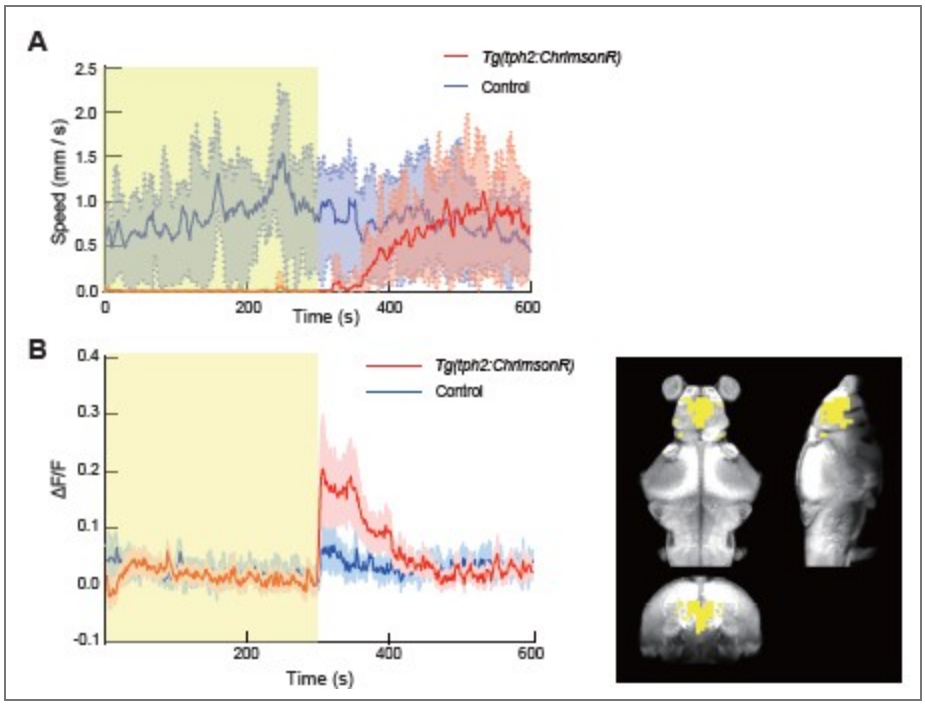

Author response image 1. Forebrain activity increases following termination of DRN optogenetic stimulation. (A) Following the termination of optogenetic stimulation of DRN 5-HT neurons, locomotor speed in Tg(tph2:ChrimsonR) zebrafish gradually recovered and returned to control levels. (B) Neural activity in forebrain regions showed a transient increase immediately after stimulation offset and gradually returned to baseline as locomotor activity recovered. discuss these possibilities. In particular, it would be interesting to examine the recruitment of regions not directly stimulated but known to be associated with other neuromodulatory systems or promoting glial activation (e.g., the locus coeruleus).

We thank you for this important suggestion. In the revised Discussion, we now frame our findings in relation to several candidate mechanisms.

Our results are most consistent with a direct neuromodulatory action of serotonin on downstream motor-related circuits. This is supported by the known projection patterns of DRN 5-HT neurons [4], which target midbrain and hindbrain regions involved in motor control, as well as by prior serotonin imaging studies showing elevated 5-HT levels in hindbrain regions during low-motor states, where inhibitory HTR1-family receptors are enriched [5]. In addition, recent voltage imaging studies have shown that DRN serotonergic neurons are embedded within a broader motor-state-dependent circuit, in which they are dynamically regulated by local GABAergic inputs [6]. We have incorporated a discussion of these potential mechanisms into the revised Discussion.

> ***Reviewer #2 (Recommendations for the authors):***
>
> *(1) Lines 91-97 page 2.*
>
> *"dPCA separates neural population activity into components tied to specific experimental variables, allowing us to isolate DRN-dependent changes (Methods). Components associated with DRN activation explained significantly more variance in Tg(tph2:ChrimsonR) zebrafish than in controls (Fig. 3A), indicating a strong serotonergic impact on brain-wide neural activity. The small stimulation-related variance in controls likely reflected visual responses to laser."*
>
> *Directly stimulated neurons are not included, as stated in the Methods, but I think it would be better to mention this explicitly in the main text.*

We thank you for this helpful suggestion. We agree that explicitly stating this point in the main text improves clarity. In our analysis, neurons directly stimulated by the laser were excluded (as described in the Methods) to ensure that the identified components reflect whole brain responses rather than direct optogenetic activation. We have now added a clarifying sentence in the Results section to make this explicit.

> *(2) Lines 113 - 115 page 3.*
>
> *"To examine how DRN 5-HT neuron activation affects sensorimotor processing (Fig. 4C), we next recorded whole-brain neural activity in head-fixed, tail-free larvae embedded in agarose to capture transient calcium signals with minimal motion artifacts."*
>
> *Lines 117-119 page 3.*
>
> *"Because head-fixed larvae rarely enter natural sleep, we applied 1 mM mepyramine, a sleep-promoting antihistamine, to induce a sleep-like state (41), which markedly changed auditory responses (Fig. 4E, Fig. S2C)"*
>
> *Why not perform these experiments in freely moving fish instead? To what extent do movements in freely moving animals affect segmentation? Is it actually problematic to apply dPCA in that case? You used it in the previous section.*

We thank the reviewer for raising this important point. In principle, freely moving preparations would provide a more natural behavioral context. However, reliable application of dPCA requires stable neuron identification and accurate trial alignment across time, both of which are substantially compromised in freely moving larvae due to motion-induced imaging noise and segmentation errors.

In our hands, whole-brain calcium imaging in freely moving fish introduces significant variability in segmentation and signal extraction, which in turn leads to unstable and noisy low-dimensional decompositions, preventing robust estimation of task-related components. By contrast, the head-fixed preparation enables consistent neuron tracking and precise alignment to sensory stimuli, which are critical for dPCA.

We have now clarified in the manuscript that all dPCA analyses were performed on head-fixed animals.

> *(3) Line 117 page 3.*
>
> *Why do you use cosine similarity? Are the results different when using other metrics?*
>
> *I can see the matrix, but what exactly are you looking for in it to support the claim "DRN activation preserved the structure of the auditory population code"? I think explaining some of these concepts more clearly, or at least providing expectations or interpretations for the different metrics and analyses, would make the manuscript easier to follow.*

We thank you for this question. Cosine similarity is widely used to quantify similarity between population activity patterns because it captures relative activity across neurons while ignoring overall gain.

In our analysis, each trial is a population activity vector, and the cosine similarity matrix encodes pairwise relationships between these vectors. We assess preservation of the auditory population code by testing whether this similarity structure (i.e., the geometry of population responses) remains consistent across conditions. We have expanded the text to clarify how these matrices are constructed and interpreted.

In addition, we computed alternative similarity measures based on Pearson correlation, which is equivalent to the cosine similarity of two vectors after they have been centered

(subtracting the mean of each vector) (Author response image 2A). We further quantified pairwise trial distances using the Euclidean chord distance on the unit hypersphere, defined as

$D_{ij} = \sqrt{2}(1-C_{ij})$, where C_{ij} is Pearson correlation; smaller distances indicate higher similarity (Author response image 2B). Both alternative measures yielded qualitatively consistent results, showing that DRN 5-HT neuron activation preserves the similarity structure across trials.

> *(4) Figure 4D.*
>
> *If "significant alignment between DRN activation and motor-related neural subspaces, with the sound related subspace being nearly orthogonal" is correct, shouldn't there be some visible overlap between blue and red, and little to no overlap with yellow? This is not easy to see. Perhaps plotting all three in a single panel would help.*

We thank you for this helpful suggestion. We would like to clarify that the "alignment" we refer to is defined in terms of the angle between neural subspaces, rather than the spatial overlap of neurons. In other words, significant alignment indicates that the corresponding population activity patterns occupy similar directions in a high-dimensional activity space.

As a result, even statistically significant aligned subspaces (see further exposition below) do not necessarily involve overlapping sets of neurons with large PC weights. This distinction is important because subspace geometry is defined at the population level and cannot be directly inferred from spatial overlap in low-dimensional visualizations. In addition, the visualization shown in Fig. 4D highlights only brain regions containing neurons with relatively high weights for illustrative purposes.

We also note that the current visualization is based on a maximum intensity projection of a 3D volume, which can create the appearance of overlap in two dimensions even when the underlying neurons are spatially segregated in three dimensions. To provide a clearer spatial reference, we have re-plotted the three subspaces in a three-dimensional representation.

> *(5) Figure 4F.*
>
> *Do the arrows represent the values for each combination? This is not clear to me. Perhaps it could be clarified in the paragraph. Most of the values, including those being compared, are around 87 plus minus 2 degrees, i.e., mostly orthogonal. Does this imply no overlap between patterns (again, this is hard to see in Figure 4D)? The values are different from the null model but still close to orthogonal. The phrase "significant alignment between DRN activation and motor-related neural subspaces" could be interpreted as strong alignment, but the values do not seem to support that, do they?*

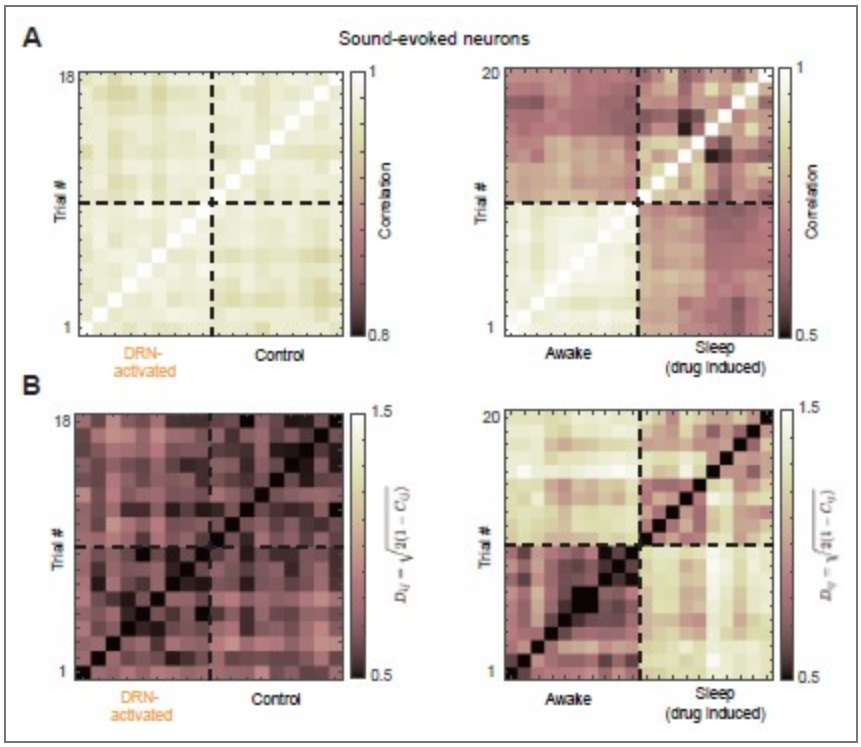

Author response image 2. Alternative similarity measures reveal preserved trial-to-trial similarity structure. (A) Trial-by-trial similarity matrix quantified using Pearson correlation. Higher correlation indicates greater similarity between trials (B) Pairwise trial distances quantified using the Euclidean chord distance on the unit hypersphere ($D_{ij} = \sqrt{2}(1-C_{ij})$), where smaller distances indicate greater similarity between trials.

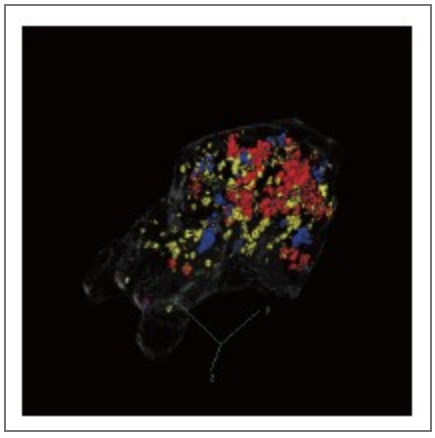

Author response image 3. Three-dimensional visualization of DRN activation-, motor-, and sound-related subspaces. Threedimensional rendering of the high-weight neurons in the DRN 5-HT activation, motor-related, and sound-related subspaces. Colors are consistent with Figure 4D.

We thank the reviewer for this important clarification.

We agree that the phrase “alignment” could be interpreted as implying strong spatial overlap in the anatomical space, which is not what we intend to convey. In our analysis, “alignment” refers to a statistically significant deviation from a null distribution.

In high-dimensional spaces, random vectors are expected to be nearly orthogonal, with angles tightly concentrated around 90°. To demonstrate this phenomenon, we conducted simulations using random vectors over a range of dimensionalities (100–10,000 dimensions)

and observed that the expected angle distribution over 1000 trials becomes progressively more concentrated around 90° as the dimensionality increases (Author response image 4). Therefore, even modest deviations from 90° reflect a systematic bias and indicate structured overlap beyond chance. So, "significantly aligned" means the motor–DRN angle is significantly less than the random baseline, and "significantly orthogonal" for sound–DRN means the angle is significantly closer to 90° than the random baseline. We will revise the text to clarify this point and avoid potential misinterpretation.

Regarding Figure 4D, we agree that the meaning of the arrows was not sufficiently clear. The arrows represent the mean angle, computed across all fish, between the DRN 5-HT activation subspace and the motor-related subspace (left), and between the DRN 5-HT activation subspace and the sound-related subspace (right). We will update the figure legend to explicitly define these elements.

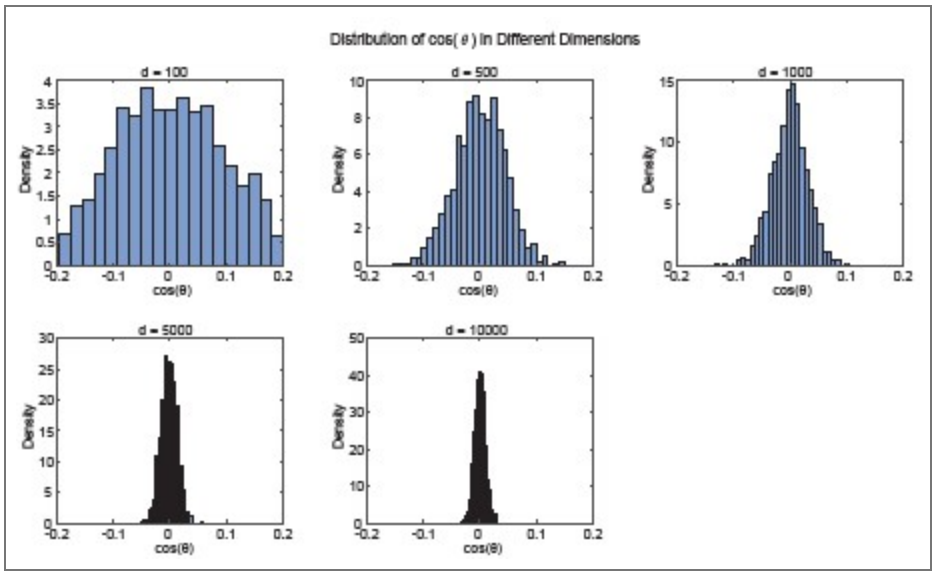

Author response image 4. Random vectors become increasingly orthogonal in high-dimensional spaces. Simulated distributions of pairwise angles between random vectors across different dimensionalities (100–10,000 dimensions; 1000 repetitions per dimensionality). As dimensionality increases, the angle distribution becomes increasingly concentrated around 90°.

> *(6) Lines 125 - 126 page 5.*
>
> *"After detecting bouts, we computed each bout's direction and amplitude and classified them into 12 types."*
>
> *It would be interesting to see how the distribution of bouts looks in the direction-amplitude space, in order to better visualize the 12 bout types (perhaps using different colors). It might also be useful to include examples of the 12 bout types in the supplementary material.*

We thank you for this helpful suggestion. To better visualize the distribution of bouts and the definition of the 12 bout types, we have added a new supplementary figure showing the distribution of all bouts in the direction–amplitude space, with each bout color-coded according to its assigned category, consistent with the scheme used in the main text.

We further quantified the frequency of each bout type across the dataset, which comprises 1,493 bouts from 7 animals. Among these, 4 animals exhibited all 12 bout types and were

therefore included in subsequent regression analyses that require complete coverage of all categories.

In addition, we have included examples of representative bout types in the supplementary material. These additions improve the clarity and interpretability of the bout classification scheme.

> *(7) Lines 131 - 133 page 5.*
>
> *"Some neurons exhibited activity related to all bout types with similar amplitudes, yielding low coefficient variability, whereas others responded selectively to specific bout types - typically those with larger tail amplitudes and turning angles - exhibiting higher variability in regression coefficients (Fig. 5B)."*
>
> *I would appreciate some quantification of "typically."*

We thank you for this suggestion. Fig. 5B (bottom) shows a neuron with large variability in regression coefficients across bout types, quantified by the coefficient of variation (CV). Bout types with large amplitudes and turning angles (e.g., type 12) have larger regression coefficients than others. We will remove "typically" from the text.

> *(8) Lines 546 - 547 page 15.*
>
> *"Fish whose baseline tail movements were insufficient to cover all 12 bout types were excluded from further analysis."*
>
> *It would be useful to report the number or proportion of animals that did not exhibit all 12 bout types. Which types of bouts are less frequently observed?*

Thank you for this helpful suggestion. In the full dataset (n = 7 fish), 4 animals exhibited all 12 bout types. We have now added a supplementary figure showing the occurrence probability of each bout type across all animals.

> *(9) Line 147 page 5.*
>
> *Honestly, the Bayesian multi-dimensional scaling is difficult to follow, and it is not clear what new insight it provides. I assume that "hyperbolic geometry indicates complex hierarchical organization" is the main point, but its meaning in this context is not sufficiently explained. This paragraph would benefit from being rewritten for clarity or potentially removed if it does not contribute essential information.*

We appreciate your insightful comments. In response, we have substantially expanded the section on Bayesian multidimensional scaling. First, we now provide an intuitive exposition (see Figure S6) of hyperbolic geometry and multidimensional scaling, clarifying why this framework constitutes a powerful approach for uncovering the geometric and functional organization of neuronal populations. Second, we show that multidimensional scaling in a curved hyperbolic space more accurately captures the correlation structure among neurons than embeddings in a flat Euclidean space. Third, and most notably, we find that the inferred curvature of the hyperbolic embedding space tightly scales with the degree of quiescence: fish in which dorsal raphe nucleus (DRN) stimulation nearly abolished locomotor activity exhibit the largest curvatures (new Figure 5F). Collectively, these computational analysis indicate that the curvature of the embedding space serves as a quantitative signature of the quiescent state.

References

(1) J. C. Marques, M. Li, D. Schaak, D. N. Robson, J. M. Li, Internal state dynamics shape brainwide activity and foraging behaviour. Nature 577, 239–243 (2020).

(2) V. Choudhary, C. R. Heller, S. Aimon, L. de Sardenberg Schmid, D. N. Robson, J. M. Li, Neural and behavioral organization of rapid eye movement sleep in zebrafish. bioRxiv pp. 2023–08 (2023).

(3) Y. Zhao, C.-X. Huang, Y. Gu, Y. Zhao, W. Ren, Y. Wang, J. Chen, N. N. Guan, J. Song, Serotonergic modulation of vigilance states in zebrafish and mice. Nature Communications 15, 2596 (2024).

(4) Z. Song, C.-X. Huang, H. Zhang, C. Ye, N. Guan, J. Song, Integrated single-cell atlases unveil the operation principles of whole-brain 5-ht neuronal subsystems. Science Advances 11, eadv8128 (2025).

(5) R. Haruvi, R. Barbara, I. Shainer, A. Rosenberg, L. Moshe, D. Malamud, J. Toledano, D. Braun, H. Baier, T. Kawashima, Global and compartmentalized serotonergic control of sensorimotor integration underlying motor adaptation. BioRxiv pp. 2024–09 (2024).

(6) T. Kawashima, Z. Wei, R. Haruvi, I. Shainer, S. Narayan, H. Baier, M. B. Ahrens, Voltage imaging reveals circuit computations in the raphe underlying serotonin-mediated motor vigor learning. Neuron (2025).

https://doi.org/10.7554/eLife.110370.2.sa0